PHOTOELECTROCHEMICAL ACTIVITY OF TITANIUM DIOXIDE THIN FILMS

by

AIDA MEHDINEZHAD ROSHAN

Presented to the Faculty of the Graduate School of

The University of Texas at Arlington in Partial Fulfillment

of the Requirements

for the Degree of

MASTER OF SCIENCE IN MATERIALS SCIENCE AND ENGINEERING

THE UNIVERSITY OF TEXAS AT ARLINGTON

May 2013

Copyright © by Aida Mehdinezhad Roshan 2013

All Rights Reserved

ACKNOWLEDGEMENTS

I would like to thank all of those who have helped and supported me in any respect during my master's degree study and research. Foremost, I would like to express my sincere gratitude to my advisor Dr. Efstathios. I. Meletis for his excellent research advices, instructions, patience, and his constant encouragement. I also want to acknowledge my outstanding committee members Dr. F. Liu and Dr. K. Rajeshwar for their time and suggestions.

I also wish to thank my friends Dr. Csaba Janaky, Dr. Cristian Cionea, Jessica Mooney, Minghui Zhang, Adam Smith, and Sujay Bagi for all of their help and support during this research project.

Further, I would like to mention the various UTA laboratories that helped in this research, Surface and Nano Engineering Laboratory (SaNEL), Characterization Center for Materials and Biology (CCMB), and Prof. K. Rajeshwar's laboratory in Chemistry & Biochemistry Department.

Finally, and most importantly, I would like to thank my parents for bringing me strength and confidence. Without their love, support and understanding, I could never have been able to make it this far.

December 18, 2012

ABSTRACT

PHOTOELECTROCHEMICAL ACTIVITY OF

TITANIUM DIOXIDE THIN FILMS

Aida Mehdinezhad Roshan, MS

The University of Texas at Arlington, 2013

Supervising Professor: Efstathios. I. Meletis

Titanium dioxide (TiO_2) is considered as an oxide semiconductor with several unique properties, including environmental sensing capabilities, biocompatibility and photocurrent generation, long-term stability, cost efficiency, and chemical inertness. TiO_2 thin films have a wide range of applications in dye-sensitized solar cells.

TiO_2 films have been deposited on two different substrates, aluminum and titanium. Two different methods used for deposition of the thin films namely: Plasma Electrolytic Oxidation (PEO) and Physical Vapor Deposition (PVD). In order to study the effect of roughness of the substrate on photocurrent generation of the deposited films, one group of substrates were “patterned” by Electrolytic Plasma Processing (EPP) prior to deposition. A “hill and valley” morphology was observed on the uppermost layer of the EPP-treated substrates. The microstructure and also roughness of the EPP-treated substrates were characterized by Scanning Electron Microscopy (SEM) and Profilometry.

Similarly, the deposited TiO_2 thin films were also characterized by SEM, Energy Dispersive Spectroscopy (EDS), Raman, Transmission Electron Microscopy (TEM), X-ray Diffractometry (XRD), and Profilometry.

It was found that the PEO deposited film on titanium substrate was composed of anatase and the film on the aluminum substrate was amorphous. The average thickness of the PEO deposited films was about 6-10 microns. TiO_2 thin films deposited by DC magnetron sputtering were found to be almost amorphous with an average thickness of 650 nm. High resolution TEM analysis showed some areas of crystallinity with a grain size of ~5 nm.

Photoelectrocurrent measurements were then performed on all deposited films by a standard single-compartment, three-electrode electrochemical cell. It has been observed that the films deposited by PVD technique have a much higher quality and produce much higher photocurrent comparing to ones of PEO method

TABLE OF CONTENTS

ACKNOWLEDGEMENTS iii

ABSTRACT iv

LIST OF ILLUSTRATIONS ix

LIST OF TABLES xii

Chapter Page

1. INTRODUCTION 1

2. OBJECTIVE 3

3. REVIEW OF LITERATURE 4

3.1 Titanium Dioxide Thin Films 4

3.1.1 Plasma Spraying 4

3.1.2 Electroplating 5

3.1.3 Electrolytic Plasma Processing 6

3.1.3.1 Phenomenology 7

3.1.3.4 Plasma Interaction with Material Surface 10

3.1.4 Magnetron Sputtering 13

3.1.4.1 Phenomenology 14

3.1.4.2 TiO_2 Coatings by Magnetron Sputter Deposition 16

3.2 Photoelectrocurrent Measurement 17

3.2.1 Semiconductors and Electric Excitation 18

3.2.2 Photocatalysis of TiO_2 21

3.2.3 Mechanism of TiO_2 Based Heterogeneous Photocatalysis 24

3.2.4 Photocurrent Measurement Techniques 25

4. EXPERIMENTAL 27

4.1 Materials 27
4.2 Experimental Setup and Deposition Conditions 28
4.2.1 Electrolytic Plasma Processing 28
4.2.2 DC/RF Magnetron Sputtering 31
4.3 Characterization of Produced Materials 35
4.3.1 Photocurrent Measurement 35
4.3.2 Surface Morphology and Roughness Measurement 36
4.3.3 Scanning Electron Microscopy 37
4.3.4 X-Ray Diffraction 37
4.3.5 Transmission Electron Microscopy 37
4.3.6 Raman Spectroscopy 38
5. RESULTS AND DISCUSSION 39
5.1 EPP Surface Patterning 39
5.1.1 SEM 39
5.1.2 Profilometry 42
5.2 PEO Coatings 42
5.2.1 Photoelectrocurrent Measurement 43
5.2.2 X-ray Diffractometry 44
5.2.3 SEM 47
5.2.4 Profilometry and Roughness Measurement 52
5.2.5 Raman Spectroscopy 59
5.3 Magnetron Sputtering Coatings 61
5.3.1 Photoelectrocurrent Measurement 62
5.3.2 EDS 65
5.3.3 TEM 66
6. CONCLUSION 73

REFERENCES 74

BIOGRAPHICAL INFORMATION 77

LIST OF ILLUSTRATIONS

Figure Page

3-1 Plasma spraying system. [13] 4

3-2 Typical setup for electroplating. 6

3-3 Electrode processes in electrolysis of aqueous solution. [17].......... 7

3-4 The two type of current-voltage diagrams for plasma oxidation processes;
(a) at the near electrode area, (b) at the dielectric film on the electrode surface. [17].... 8

3-5 Schematic of the EPP process mechanism showing one single plasma bubble:
(a) plasma bubble on the surface of the work piece,
(b) shockwave production by the cooling plasma bubble,
(c) collapsing plasma bubble and cleaning,
(d) collapsing plasma bubble and creation of micro-crater,
(e) collapsing bubble deposits ions in case of coating, and
(f) increasing coating thickness with processing time. [24] 11

3-6 Schematic representation of sputtering system. [31] 15

3-7 Schematic photoexcitation and deexcitation in solid. [41].......... 19

3-8 Relative dispositions of various semiconductor band edge positions
shown both on the vacuum scale and with respect to the SHE reference.
These band edge positions are for an aqueous medium of pH ~1. [41] 20

3-9 Crystalline structures of different types of titanium oxides.
(http://ruby.colorado.edu/~smyth/min/tio2.html) 23

3-10 Linear sweep photovoltammograms with 0.1 Hz chopped irradiation
of a nonporous TiO_2 film obtained by anodization of Ti foil. [59] 26

4-1 CAP Technologies EPP reactor that was designed to handle
different types of specimens. [13].......... 29

4-2 EPP reactor and setup built at UTA;
right side image represents the close up view of the reactor. [13] 30

4-3 Schematic representation of the home built
hybrid plasma CVD and PVD system. [60].......... 32

4-4 Hybrid plasma CVD and PVD system
(a) Front view of the system, (b) Side view of the system. [60].......... 34

4-5 Schematic principal of photoelectrocurrent

measurement by linear-sweep voltammetry 36

5-1 Top surface SEM micrographs of EPP-treated 1100 Al at different processing times of (a) 10 s (b) 20 s, and (c) 30 s. [13] 40

5-2 Top surface SEM micrographs of EPP-treated pure Ti at different processing times of (a) 10 s (b) 20 s, and (c) 30 s. [13] 41

5-3 R_a as a function of processing time. [13] 42

5-4 Photoelectrocurrent activity of T (flat Ti substrate coated with TiO_2) and PT (EPP cleaned Ti substrate coated with TiO_2). 44

5-5 XRD pattern of A (Flat Al substrate coated by TiO_2). 45

5-6 XRD pattern of PA (EPP treated Al substrate coated by TiO_2). 45

5-7 XRD pattern of T (Flat Ti substrate coated by TiO_2). 46

5-8 XRD pattern of PT (EPP treated Ti substrate coated by TiO_2). 46

5-9 The microstructure of flat Ti substrate coated with TiO_2 (T) at different magnifications. 48

5-10 The microstructure of EPP treated Ti substrate coated with TiO_2 (PT) at different magnifications. 49

5-11 The microstructure of flat Al substrate coated with TiO_2 (A) at different magnifications. 50

5-12 The microstructure of EPP treated Al substrate coated with TiO_2 (PA) at different magnifications. 51

5-13 Average roughness of TiO_2 thin film on flat and EPP treated samples. 52

5-14 Three-dimensional topography of TiO_2 thin film on flat and EPP treated Al substrates. 54

5-15 Three-dimensional topography of TiO_2 thin film on flat and EPP treated Ti substrates. 55

5-16 Two-dimensional topography of the surface of T. 56

5-17 Two-dimensional topography of the surface of PT. 57

5-18 Two-dimensional topography of the surface of A. 58

5-19 Two-dimensional topography of the surface of PA. 59

5-20 Raman spectra of TiO_2 thin film on flat Ti substrate (T). 60

5-21 Raman spectra of TiO_2 thin film on EPP treated Ti substrate (PT). 60

5-22 Raman spectra of TiO_2 thin film on Al substrate (A). 61

5-23 Linear-sweep photovoltammograms of
sputtered TiO_2 thin film on flat Al substrate (SA). 63

5-24 Linear-sweep photovoltammograms of
sputtered TiO_2 thin film on EPP treated Al substrate (SPA). 63

5-25 Linear-sweep photovoltammograms of
sputtered TiO_2 thin film on EPP treated Ti substrate. 64

5-26 Linear-sweep photovoltammograms of
sputtered and PEO TiO_2 thin film on Ti substrate. 65

5-27 EDS spectra of TiO_2 thin film on Al substrate. 66

5-28 TEM micrograph of the sputtered TiO_2 thin film. 67

5-29 High resolution TEM image of the sputtered TiO_2 thin film. 68

5-30 TEM ring pattern of the sputtered TiO_2 thin film on amorphous carbon. 68

5-31 TEM ring pattern of the sputtered TiO2 thin film on amorphous carbon
after annealing at 450°C for 2 hours. 70

5-32 High resolution TEM image of the sputtered TiO_2 thin film
after annealing at 450°C for 2 hours. 70

5-33 Linear-sweep photovoltammograms of sputtered Al substrate
after annealing at 450°C for 2 hours. 72

LIST OF TABLES

Table Page

3-1 Properties of Different Types of Titanium Oxide 22

4-1 Codes of Samples According to Substrates and Method of Coating 28

5-1 Atomic and Weight Percent of Each Element in TiO_2 Thin Film 66

5-2 Anatase and Rutile D-Spacing 72

CHAPTER 1

INTRODUCTION

Oxide semiconductors have attracted the attention of researches due to their variety of applications. Among different types of these semiconductors, TiO_2 has many unique properties including environmental sensing capabilities, biocompatibility and photocurrent generation [1]. It is also considered to be cost effective, long-term stable, and chemically and biologically inert [2]. There has already been a wide range of applications for TiO_2 such as photodecomposition of waste sewage, air purification, self-cleaning windows, sensors, photovoltaic devices and biocompatible treatment for implants. Many of these noble properties of TiO_2 are mainly due to relatively high surface area of this oxide and also being kinetically favorable of electron-hole pair generation [1].

Many studies have tried to examine the photocatalytic activity based on TiO_2 particle size suggesting an increase in photocurrent activity of the semiconductor with a decrease in the particle size [3]. Similarly, regarding the morphology of titanium dioxide thin films, studies have stated that the photoactivity of the film increases as the roughness increases [4]. For example, a three-dimensional porous structure of TiO_2 with a large surface area is known to exhibit an enhanced photocatalytic performance [2]. On the other hand, in spite of so many important developments in nano-structural engineering for TiO_2 films, detailed microstructural observations and characterization have rarely been carried out.

The above-mentioned importance of size and morphology effect of TiO_2 particles and TiO_2 films has led to efforts to develop such thin films with methods that can produce the desirable roughness. There has been several studies trying to deposit TiO_2 films on titanium substrates; however, titanium is a rather expensive metallic substrate. Therefore the current study tries to produce such thin films on a cheaper substrate. Aluminum metallic substrate was

chosen to be coated by TiO_2 films as well as titanium substrates. TiO_2 has been synthesized by different techniques including sol-gel [5], chemical and physical vapor deposition (PVD) [6-7], hydrothermal process [8], electrochemical methods [9], and liquid phase deposition [10]. It can also be obtained via plasma electrolytic oxidation (PEO), also known as Micro Arc Oxidation (MAO). PEO is an electrochemical technique for formation of anodic films by spark/arc micro-discharges, which move rapidly on the vicinity of the anode surface [11]. The PEO process is carried out at voltages higher than the break down voltage of the gas layer around the substrate (anode). Therefore, there will be formation of electrical discharges around that gas layer. The PEO process is mainly characterized by these sparks leading to the formation of different ceramic films. The PEO technique is the first method that has been used to develop thin films in the current study.

Another technique used to develop TiO_2 thin films in the current study is DC magnetron sputtering. It is a promising method to create thin films with a high quality and high adhesion to the substrate. Nanocrystalline films can be developed by this method and many different parameters enable one to control the morphology, thickness and also roughness of the film.

In the present study, TiO_2 thin films were developed by the PEO method and also PVD on Ti and Al substrates. The produced films were characterized and their photoelectrocurrent activity was measured.

CHAPTER 2

OBJECTIVE

Crystalline titanium dioxide (TiO_2) thin films have been extensively investigated due to their various applications in a wide range of fields such as photocatalysis, solar cells, gas sensors, self-cleaning windows, etc.

The main objective of this study is to deposit TiO_2 thin films not only on Ti substrates, but also on inexpensive Al substrate to measure the photoelectrocurrent. One main target of the study is to compare the quality of TiO_2 thin films deposited by PEO and PVD in terms of photocurrent production. On the other hand, roughness of different TiO_2 thin films and its effect on photoelectrocurrent is to be studied as well. The goal of the current study is to acquire TiO_2 thin film in anatase phase, which has the highest photoactivity, and get the highest photoelectrocurrent on both Ti and Al substrate using PEO and PVD as two different deposition techniques.

CHAPTER 3

REVIEW OF LITERATURE

3.1 Titanium Dioxide Thin Films

There are several techniques applied to produce thin films. Most of these techniques could be applied to obtain titanium dioxide thin films. Some of these methods are being discussed in this chapter.

3.1.1. Plasma Spraying

In general, plasma spraying [12] is a thermal activated method of coating in which melted material is sprayed onto the substrate by plasma jet. The jet is heated up to 10,000 K and the melted material is propelled toward the substrate and solidifies there. Figure 3-1 shows the schematic of this technique.

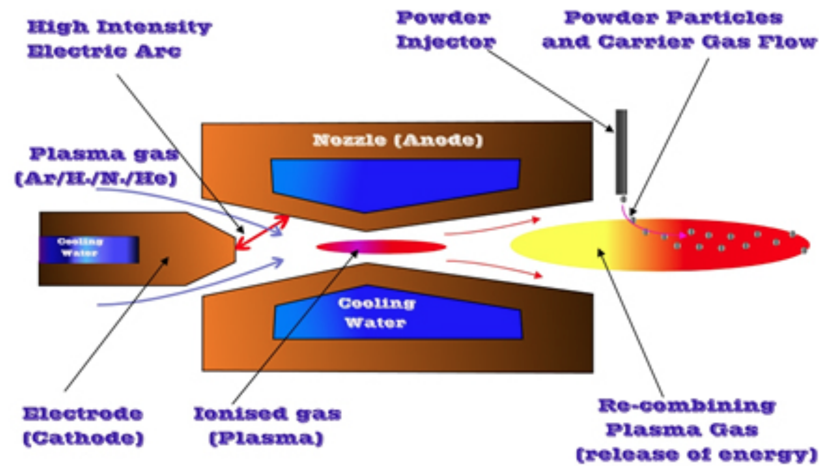

Figure 3-1 Plasma spraying system. [13]

There are many different types of plasma spraying systems characterized based on foaming media (hydrogen, argon, helium), spraying environment (air or vacuum), and plasma jet power generation (DC or RF plasma).

Coatings created by this method are generally used for protection against high temperatures, wear, erosion, and corrosion barriers. The deposited film consists of multiple pancake-like lamellae formed by solidification of droplets of melted materials. Therefore, there are always small cores or cracks or porosities in these types of thin films. As a result, these deposited films always have significantly different properties from bulk materials such as lower strength, conductivity and modulus.

There have been previous studies on deposition of TiO_2 coatings by the plasma spraying method [14].

3.1.2. Electroplating

Electroplating is a coating process in which metal ions existing in the solution are moved by an electric field toward an electrode. Using electrical current during the plating reduces cations of a desired material from the electrolyte and coats the conductive substrate with a thin film. The electroplating process is mainly used for enhancing the properties of a film for purposes such as corrosion protection, rear resistance, and etc., and also for increasing the thickness of undersized parts [15].

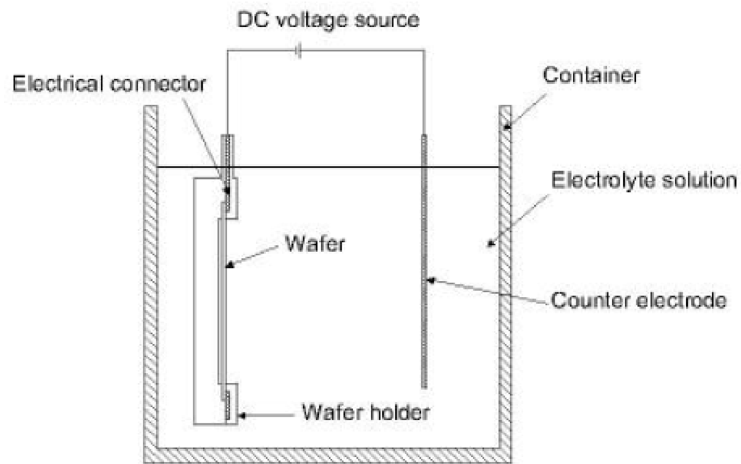

Figure 3-2 Typical setup for electroplating.

Figure 3-2 shows a typical setup for a regular electroplating system. The electrodeposition process is actually a reversed galvanic cell, meaning that the part to be plated is the cathode in the circuit. Both the anode and the cathode are immersed into the solution and dissolved metal salts and other ions provide the conductivity. Plating quality and also deposition rate can be controlled by current density. Several attempts had been made to coat material with titanium dioxide by electrodeposition [15]. However, this method is not totally an environmental friendly technique and is to be replaced by other methods such as PVD.

3.1.3. Electrolytic Plasma Processing

EPP is a relatively new technique used for cleaning metal surfaces and also deposition. This method can be categorized into two different processes, cathodic and anodic. The cathodic process is used for cleaning the surfaces and removing impurities. It also creates certain textures on the surface while cleaning it. On the other hand, the anodic process is known as PEO, which is used for coating by oxides. There have been several efforts on growing thin films on metal surfaces using PEO.

The general mechanism of PEO is based on the two following characteristic phenomena: First, the application of a potential between the work-piece (metal) and a counter-

electrode, leading to electrolysis of the liquid environment; and second, the production of an electrical discharge at the work-piece surface [16].

3.1.3.1 Phenomenology

It is well known that in electrolysis of an aqueous solution, the anodic surface is the place where the liberation of gaseous oxygen and/or metal oxidation occurs on. This oxidation process can lead either to surface dissolution or to oxide film formation, depending on the electrolyte chemical activity in respect to the metal's. On the other hand, liberation of the gaseous hydrogen and/or cation reduction occurs on the cathodic surface. This electrode processes in electrolysis is schematically shown in Figure 3-3.

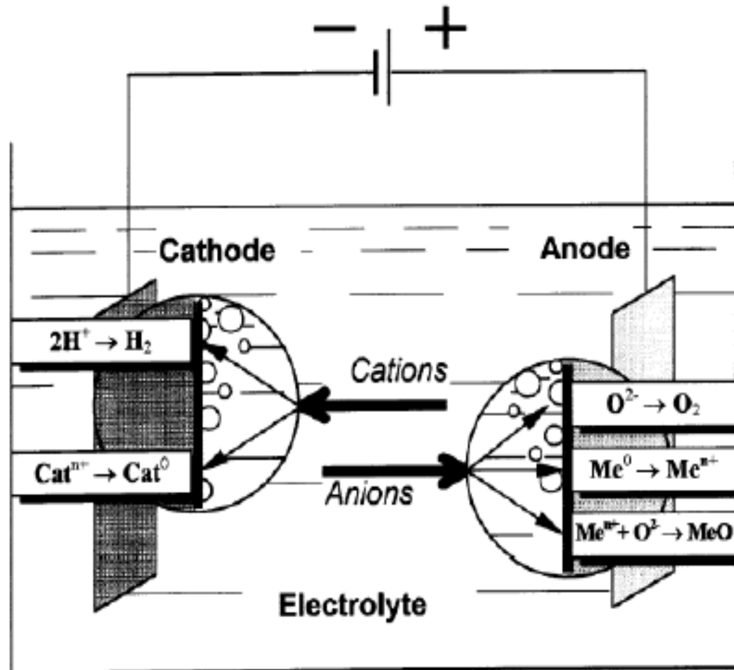

Figure 3-3 Electrode processes in electrolysis of aqueous solution. [17]

The characteristic current-voltage curve, shown in Figure 3-4 is affected by the above-mentioned processes. Type (a) current–voltage plot shows a metal–electrolyte system along with gas liberation. Type (b) represents a system formation of the oxide film.

At relatively low voltages, the kinetics of the processes occurring onto electrodes follows Faraday's law and the current-voltage relationship changes according to Ohm's law. At higher voltages, diagram (a) shows fluctuation in current, which is complemented by luminescence. At the same time, the current density keeps increasing at the areas of the substrate, which are in contact to the electrolyte, causing local boiling of the electrolyte. At the very higher voltages, the electron field reaches a very high value, which is sufficient to initiate ionization processes in the vapor envelope around the electrode. As the result of this ionization process, initially rapid sparking takes place on the surface of the substrate and after a while, the sparking transforms onto a uniform glow. At the last step, due to the hydrodynamic stabilization of vapor envelope the current drops and glow discharge changes into intensive arcing [13].

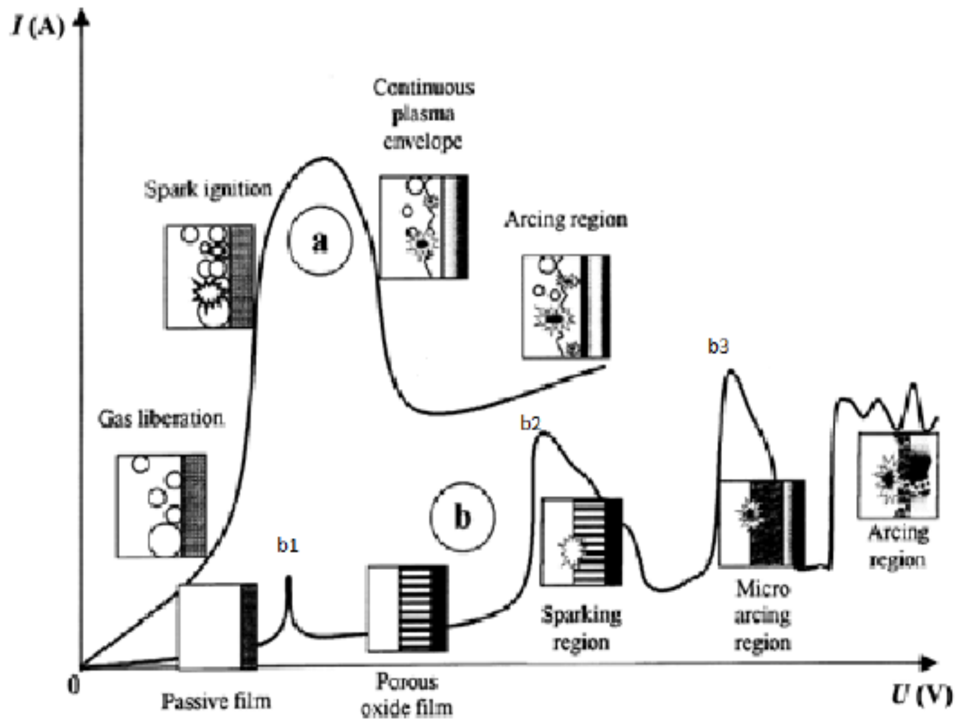

Figure 3-4 The two type of current-voltage diagrams for plasma oxidation processes; (a) at the near electrode area, (b) at the dielectric film on the electrode surface. [17]

Diagram (b) shows a different behavior in current by increasing the voltage. With a small increase in voltage up to the values corresponding to the corrosion potential of the

material, previously formed passive film begins to dissolve at point b1. Then, there will be the formation of the passive film in the repassivation region. After b2, the electric field strength in the oxide film keeps increasing to a critical value beyond which the film is broken through. This break down of the film occurs due to the impact or tunneling ionization, which leads to the formation of small sparks. From the point, b3, as the temperature increases, the mechanism of the process is also supported by the thermal ionization; therefore, slower and larger sparks will appear. The film will be gradually fused and alloyed with the elements contained in the electrolyte due to these micro-arcs. The higher voltages may cause destructive effects such as thermal cracking of the film.

According to the above-mentioned mechanism for micro arc oxidation method, the very strong adhesion and high porosity of the growing film can be justified. Since the PEO mechanism consists of several melting and solidification events of the metal surface with adsorbing electrolyte elements at the same time, the ingrowing film has a very strong adhesion to the substrate and there will just be a very small amount of volume change after coating. The high porosity of the film is due to the intense sparks on the film surface during the process.

In definition, plasma is a gas with a certain portion of ionized particles. Because of the presence of these ionized particles or charge carriers, plasma is electrically conductive, while at the same time it does not have the main properties of solids, liquids, or gases. So it is considered to be a distinct state of matter. Like gases, plasma does not have a discrete shape but under influence of a magnetic field will form structure like filaments. Plasma is characterized by its ions in presence of an electrode. Temperature controls the degree of plasma ionization. Therefore, an applied potential will accelerate plasma particles and increase the temperature. This property is being taken advantage of during ‘plasma processing” techniques, weather in aqueous or vacuum atmosphere [18].

The formation and stability of small-scale size bubbles located at the liquid-solid interface has been studied previously [19-21]. The formation of bubbles and also the size and

density of them depend on the amount of the dissolved gas, so the bubbles will disappear by degassing the solution [19]. The classical theory of bubble stability [20] expresses that in order to balance the compressive action of surface tension, the internal pressure inside the small bubbles is very high. Because of the fact that this internal pressure is much larger than the gas concentration at the other side of the bubble, there will be a diffusion process of the gas from inside the bubble to the electrolyte, leading to bubble dissipation. In order for the bubble to keep its stability against dissolution, a physical effect is needed to cancel the diffusive outflow. Stabilization can be achieved by mechanisms causing an influx of gas into the bubble. The gas enrichment near solid wall provides the best region for this influx of gas into the bubble. This phenomenon was confirmed by spectroscopy and also x-ray reflectivity measurements [22]. Considering factors, such as material properties of the solid wall and the relative gas concentration, there will be an optimum bubble size for which a dynamic equilibrium exists [23].

3.1.3.4 Plasma Interactions with Material Surfaces

The purpose of metallic coatings is to enhance the surface related material properties such as corrosion, wear, fatigue crack initiation, etc. However, the surface needs to be cleaned before coating in order for oxides and other contaminants to be removed so as to have a successful deposition and a strong adhesion between the coating and substrate.

Figure 3-5 is a schematic representation of the EPP treatment process mechanism. As mentioned before, the process time corresponds to the time during which there is stable plasma all over the work piece. In order to model the process, it is assumed that the gaseous envelope is composed of gas bubbles. The applied voltage between the electrodes is very high (about 150-200 V). This will induce concentration of positive ions from the electrolyte around the virtual bubbles formed by the hydrogen evolution from electrolysis. This high concentration of positive

charges around the cathode will generate an intense, localized electric field (about 10^5 V/m).

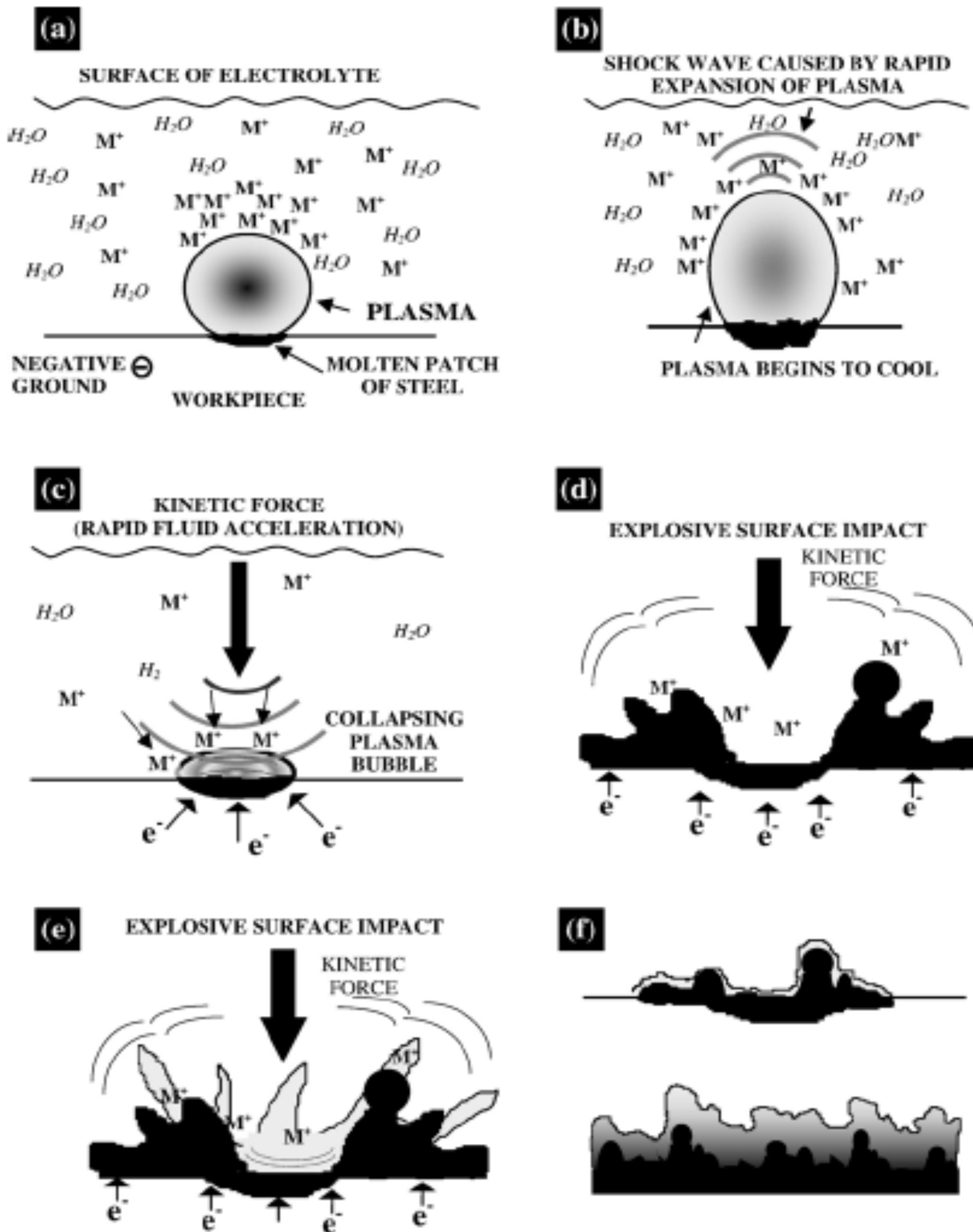

Figure 3-5 Schematic of the EPP process mechanism showing one single plasma bubble: (a) plasma bubble on the surface of the work piece, (b) shockwave production by the cooling plasma bubble, (c) collapsing plasma bubble and cleaning, (d) collapsing plasma bubble and creation of micro-crater, (e) collapsing bubble deposits ions in case of coating, and (f) increasing coating thickness with processing time. [24]

The gas inside the bubble will be ionized and become plasma due to this strong electric field. The discharge will be initiated at this step as it is shown in Figure 3-5(a). The ionization phenomena appear initially as a rapid sparking and then transforms into a uniform glow distributed all around the enveloping gaseous layer. At this time, the plasma temperature may reach to thousands of degrees [15]. The work piece has a much lower temperature though, which results in cooling than the plasma and collapsing the bubble on the electrode surface, Figure 3-5(b) to 3(d). The extinction of discharges takes place at about ~ 10^{-6} sec per each individual collapse. Recent studies on the anodic EPP revealed that discharges are individual events present at a given time, although the plasma envelope appearance is uniform around the work piece [25].

The collapse of the plasma bubble on the metal surface will lead to two phenomena: First, the metal ions present in the electrolyte near the surface will be accelerated toward the substrate surface. Second, the kinetic energy generated from collapsing of the bubble will be released onto the surface of the cathode [26]. This very high energy (order of hundreds of MPa) accelerates the movement of more ions toward the surface of the substrate, resulting in a very high rate of deposition (as high as 1 μm/s) [27]. Therefore, it can be concluded that the two main driving forces for this method of coating are: ion acceleration through the plasma and ion absorption transport. Also, hydrodynamic transport of ions, which is promoted by electrolyte flow, affects the movement. The combination of all these actions leads to a very high deposition rate.

The other important effect of the bubble collapse phenomena is for the surface to be quenched by the electrolyte environment, which leads to unique surface microstructures. As a result of very hot plasma near the surface of the substrate and also mechanical impact of the generated wave of bubble collapsing, impurities of the electrode surface will be instantly removed. At the same time, the hydrogen reduces oxides at the surface [27]. The repeating process of localized melting and bubble cavitation will cause a desirable profile with micro-

craters on the surface of the work piece. It also provides a mechanical interlocking for subsequent coating resulting a very good adhesion of the film to the substrate.

In summary, it can be concluded that deposition is the combination of three concurrent processes: acceleration of the ions through plasma, ion adsorption, and transportation of the ions to the electrode surface via bubble collapsing. On the other hand, due to the high temperature of plasma, a localized surface melting will occur on the work piece. Therefore, the deposition initially is mainly a mixing layer of substrate/coating elements, which results in a very good adhesion for the subsequent coating formation. Due to high plasma energy and very fast cooling rates, an ultrafine grain structure can form along with non-equilibrium phases at the substrate/coating interface.

EPP has the ability to routinely deposit metal and alloy coatings, such as Zn, Ni, Zn-Ni, Ni-Cu and recently to alloy metals such as Mo onto the metallic substrate [28].

3.1.4. Magnetron Sputtering

One of the commonly used methods in depositing thin films is PVD. There are three main different categories of PVD: thermal evaporation, ion plating, and sputtering; however, all of them follow these three basic steps: first of all, the material to be deposited has to be put into the vapor phase. This can be accomplished by methods such as sputtering, evaporation, or chemical gases. The next step is for the vapor species to be transported to the substrate, which, in case of sputtering occurs through creation of plasma containing ionized sputtering gas. The final step is the nucleation and growth of the coating on the substrate surface [31].

There are several advantages making PVD a unique method in thin film deposition. One of the key advantages of this method is the very good adhesion of the thin film to the substrate. This is because of sputter cleaning and also heating the substrate prior to the creation of the thin film. The other important property of PVD is the ability to control the microstructure of the film. By adjusting different parameters such as voltage, power, pressure, and etc. different micro and nanostructures can be obtained. Other advantages of this method

include relatively high purity of the deposited film due to vacuum environment of the deposition, adjustable deposition rate, uniform thickness and properties of the created film, and also low occurrence of hydrogen embrittlement comparing to other methods such as electroplating.

3.1.4.1 Phenomenology

Generally, sputtering is defined as the ejection of atoms or particles from a target toward the cathode by excitation of energetic particles near the room temperature [32]. Ejection of atoms from the target takes place in different steps. First of all, free electrons that are present inside the chamber will be accelerated away from the negatively charged cathode. Some of these accelerated electrons will then collide with the sputtering gas (such as Ar) inside the chamber, resulting in and electron and an Ar^+ ion. This positively charged Ar^+ ion will then be drawn toward the negative cathode. The target material will then get excited by the Ar^+ and sputters off. These ejected atoms or particles will then be deposited on the surface of the substrate. As this process is repeating, a number of free electrons will collide with Ar^+ ions and form Ar atoms. This causes the electron to return to its ground state, and release a photon. These released photons then result in the glowing light associated with plasma. A schematic view of this phenomenon is shown in Figure 3-6.

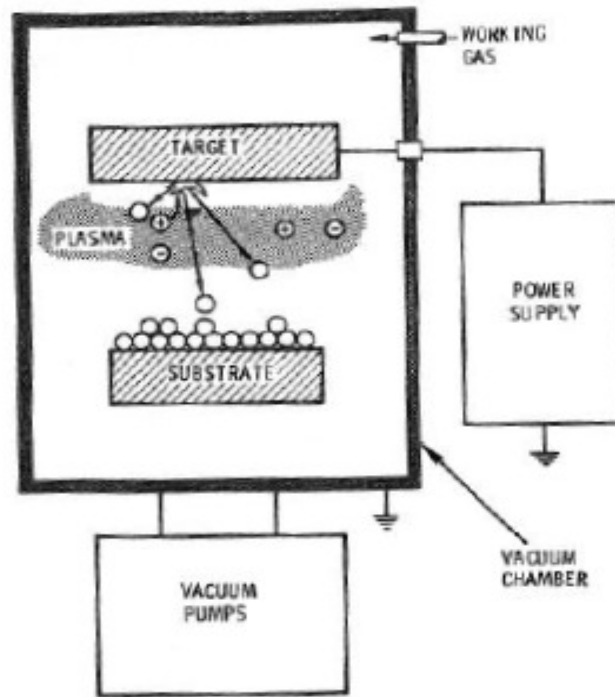

Figure 3-6 Schematic representation of sputtering system. [31]

There are however, two main negative issues about this technique. The first one is the slow deposition rate and the second one could be mentioned as a decline in quality of the deposited film. A solution for these drawbacks could be to apply a magnetic field around the cathode (target). Magnetron sputtering helps to increase both the deposition rate and the deposition quality. This applied magnetic field helps to have the electrons right above the target, thus, increases the chance of collisions between electrons and Ar atoms, leading to a higher deposition rate and also a better quality of the film. [32]

The power supply used for sputtering can be either a DC or an RF source. Usually, in case of metallic materials, a DC power is preferred and for insulating materials, RF is typically used. In either case, a number of different parameters have to be employed to obtain the desirable coating. Some of the parameters having effect on deposition composition and microstructure include the power or voltage applied to the target, the bias voltage applied to the

substrate, flow rate of sputtering gas or gasses, working pressure, target to substrate distance. Gasses such as O_2 or N_2 can also be introduced into the chamber to be incorporated into the coating material. This process is called reactive sputtering.

3.1.4.2 TiO_2 Coatings Deposited by Magnetron Sputtering

TiO_2 thin films have been widely used due to their wide range of applications such as electrochromism, photocatalysis, solar cells, gas sensors, self-cleaning windows, etc. They are one of the most promising candidates for renewable, inexpensive, efficient, and long-term energy sources. Porous TiO_2 thin films are commonly used as an anode electrode in dye-synthesize solar cells [33]. The structure of these TiO_2 thin films greatly influences the performance of cells. Researches have shown that the anatase form of TiO_2 thin films has a higher efficiency than rutile and amorphous TiO_2 [33]. On the other hand, as the surface structure becomes rougher, there will be a higher efficiency in photocurrent activity of the film. Nanostructure TiO_2 films with anatase phase can be developed using magnetron sputtering. There have been some experiments conducted in this area. TiO_2 deposition can be performed using titanium or titanium dioxide target. Both RF and DC magnetron sputtering have been used for deposition of TiO_2 films. In case of using titanium target for the deposition, oxygen gas has to be introduced to the chamber as well as argon. Oxygen is needed in order to react chemically with titanium particles from the target and deposit as TiO_2 on the substrate. Different ratio of O_2 to Ar gasses will lead to different type of TiO_2 films. As the amount of O_2 increases in the system, the film tends to be more crystalline. The other way to obtain crystalline TiO_2 films is to post-anneal the amorphous film to crystalize it. The anatase phase is only stable in temperatures less than 500°C. In case of using a TiO_2 target for deposition, no extra oxygen is needed in the chamber. In most of the cases, no preheating is needed for the substrate. Other parameters such as volume of oxygen gas, pressure, and applied power can influence the structure of the obtained film [34-39].

3.2 Photoelectrocurrent Measurement

In chemistry, photocatalysis is the acceleration of a photoreaction in presence of a catalyst. During this process, light is absorbed by a substrate. The photocatalytic activity (PCA) depends on the ability of the catalyst to create electron-hole pairs, which generates free radicals (hydroxyl radicals) able to undergo secondary reactions.

There are two types of Photocatalysis: homogeneous photocatalysis and heterogeneous photocatalysis. In homogeneous photocatalysis, the reactants and the photocatalyst exist at the same phase. But the heterogeneous photocatalysis happens when the catalyst is in different phase from the reactants. Semiconductors are the most common heterogeneous photocatalyst because of their unique characterizations. They have a void energy region on their electron structure, where no energy levels are available to promote recombination of an electron and hole produced by photoreactivation in the solid; whereas metals have continuum of electronic states. The so-called void region of semiconductors, which extends from the top of the filled valance band to the bottom of the vacant conduction band, is named the band gap. Whenever a semiconductor is struck by light, an electron in the valance band will jump to the conduction band. As a result, a positive hole will be generated. In order for photocatalyzed reaction to be favored, the recombination of the electron and the hole must be prevented as much as possible. On the other hand, it is favored to have a reaction between activated electron and the oxidant to produce reduced product and a reaction between generated holes with the reductant to produce and oxidized product. Oxidation-reduction reactions will take place on the surface of semiconductors due to the generation of positive holes and electrons at that place. The moisture has to be present on the surface of the semiconductor so as for oxidative reaction to take place and produce hydroxyl radical.

All the reactions are listed below. As it can be seen, ultimately, the hydroxyl radicals are generated in both reactions. These radicals are very oxidative in nature and non-selective with redox potential of +3.06 V [40-41].

Oxidative reactions due to photocatalytic effect:

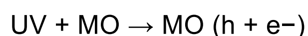

$UV + MO \rightarrow MO\ (h + e^-)$

Here MO stands for metal oxide.

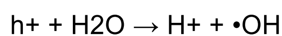

$h^+ + H_2O \rightarrow H^+ + \bullet OH$

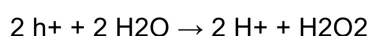

$2\ h^+ + 2\ H_2O \rightarrow 2\ H^+ + H_2O_2$

$H_2O_2 \rightarrow HO\bullet + \bullet OH$

The reductive reaction due to photocatalytic effect:

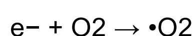

$e^- + O_2 \rightarrow \bullet O_2$

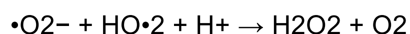

$\bullet O_2^- + HO\bullet_2 + H^+ \rightarrow H_2O_2 + O_2$

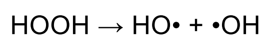

$HOOH \rightarrow HO\bullet + \bullet OH$

3.2.1. Semiconductors and Electric Excitation

In general, photocatalysis processes involve the initial absorption of photons by a molecule or substrate to produce highly reactive electronically excited state. The system's light absorption characteristics dictate the efficiency of the photoinduced chemistry. The absorption of photon radiation occurs very rapidly; however, deexcitation will always take place but in slower rates. Deexcitation of the excited molecule favors the route, but it will minimize the lifetime of the excited state. It can occur via emission of radiations such as fluorescence and phosphorescence or a radiationless decay. Therefore, the excitation lifetime always depends on the competition between excitation state and recombination [41].

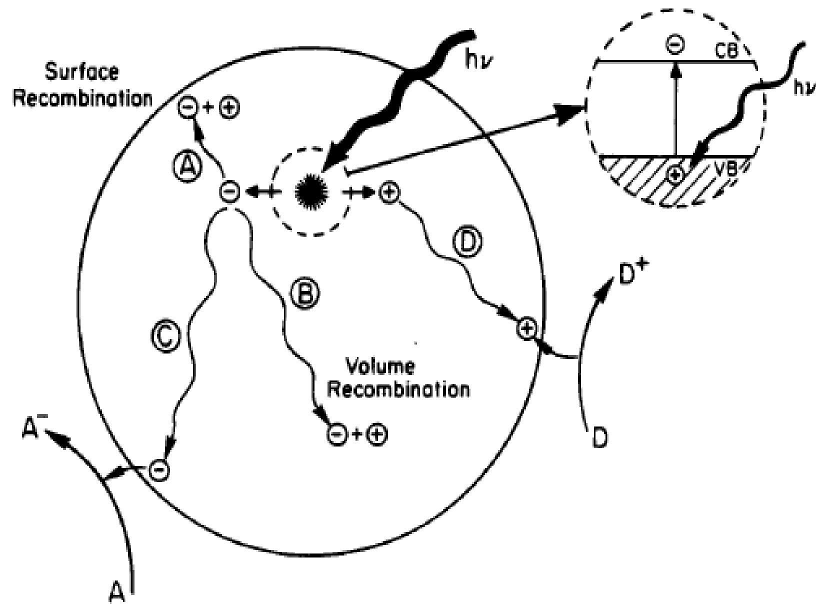

Figure 3-7 Schematic photoexcitation and deexcitation in solid. [41]

Metals have a continuum of electronic states, but semiconductors, on the other hand, possess a void energy region. There is no energy level available in this region to allow the recombination of the electron and hole produced by photoactivation. This void region that extends from the top of the filled valance bond to the bottom of the vacant conduction band is called band gap. This energy difference between the valance and conduction band determines whether the solid is a conductor, semiconductor, or an isolator. Metals have a small band gap, which enables electrons to transfer easily between the valance band and conduction band resulting in a good electrical conductivity. In case of a very large band gap, electrons will not be able to get excited and go to the valance band under normal conditions and the material becomes an insulator. Because of existence of a medium energy band gap in semiconductors, in ordinary temperatures, there are still some thermally excited electrons that grantees the conductivity. Once the excitation takes place, a positively charged vacancy will also remain in valance band, called hole. Excitation can also take place photochemically. Under such a

condition, there will be a sufficient life time for the created electron-hole pair to undergo charge transfer to adsorbed species on the surface from the solution or gas phase contact [53].

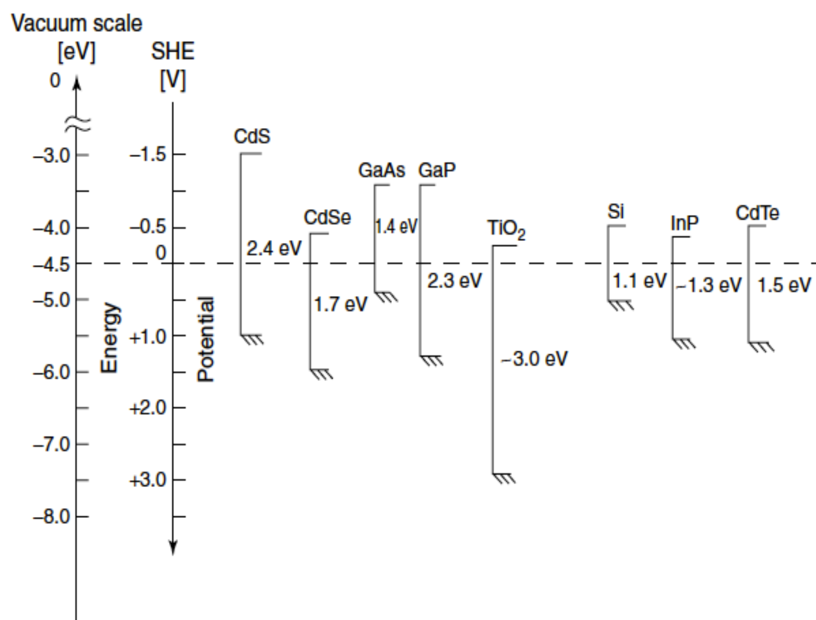

Figure 3-8 Relative dispositions of various semiconductor band edge positions shown both on the vacuum scale and with respect to the SHE reference. These band edge positions are for an aqueous medium of pH ~1. [41]

Figure 3-7 shows the excitation of an electron from the valance band to the conduction band due to irradiation of a light. The energy of this irradiated light needs to be equal or greater than the band gap of the semiconductor. Figure 3-8 shows the band edge positions of several semiconductors. These relative positions of the valance and conduction bands determine the probability and rate of charge transfer processes.

There are two factors determining the ability of a particular semiconductor to be subjected to photoinduced electron transfer: the redox potential of the adsorbate, and band gap position of the semiconductor. From the thermodynamic standpoint, when a semiconductor's condition band is higher than the acceptor's potential level, photinduced electron transfer can

happen. Moreover, the semiconductor’s valance band needs to be lower than the potential level of donor in order to give an electron to the empty hole.

The main reason that photoinduced electron transfer happens in semiconductors is that electrons and holes tend to be in contact with organic and inorganic species or the solvent. Hence, they migrate to the surface of the semiconductor. Also, when the species are preadsorbed to the surface, the process of transferring electron is more efficient [43].

3.2.2. Photocatalysis of TiO_2

Titanium oxide in nature occurs in three different crystalline forms: anatase, rutile and brookite. Anatase and rutile crystallize in tetragonal system whereas brookite crystalize in rhombic system. Table 3-1 summarizes the information about the three different polymorphs of TiO_2. Crystallographic structures of the three different oxides are shown in Figure 3-9 [60-62]. Anatase and rutile are more commonly occurring forms of TiO_2. Anatase, the meta-stable polymorph, transforms rapidly to rutile at temperatures above 700°C. The phase change from anatase to rutile has been reported to occur in different temperature ranges from 600 – 1000°C depending on the crystallite size and impurity contents [54].

Table 3-1 Properties of Different Types of Titanium Oxide

	Rutile	**Anatase**	**Brookite**
Formula weight (g/mol)	79.89	79.89	79.89
Crystal system	Tetragonal	Tetragonal	Orthorhombic
Unit cell			
a(Å)	4.5937	3.7845	5.4558
b(Å)	-	-	9.1819
c(Å)	2.9587	9.5143	5.1429
Z	2	4	8
Point group	4/mmm	4/mmm	mmm
Space group	P42/mmm	I41/amd	Pbca
Unit cell volume (Å)	62.43	136.27	257.63
Density (g/cm3)	4.25	3.89	4.133

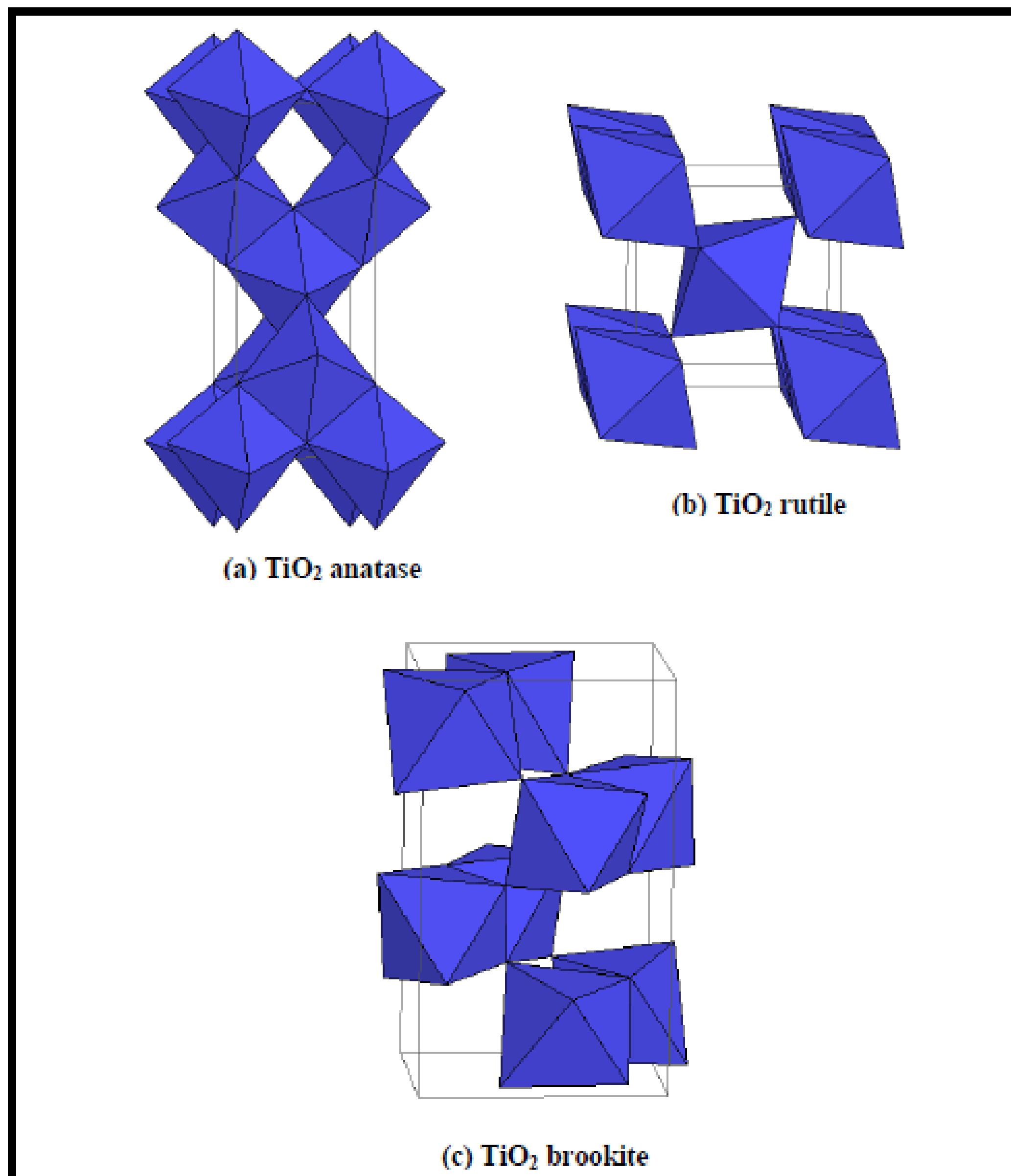

Figure 3-9 Crystalline structures of different types of titanium oxides. (http://ruby.colorado.edu/~smyth/min/tio2.html)

Both structures of anatase and rutile can be described by chains of TiO_2 octahedra. Each Ti^{4+} ion is surrounded by an octahedron of six O^{2-}. This octahedron in rutile shows a very little orthorhombic distortion, but the octahedron in anatase is significantly disordered. The number of nearest neighbors of octahedrons is also different in anatase and rutile. The anatase phase has a higher photocatalytic activity than rutile. Several factors such as the crystal structure, size distribution, porosity, band gap, band edge position, surface defects, surface hydroxyl group and surface area are enhancing photocatalytic activity in anatase [55-56]. There is a 0.2 eV band gap energy difference in anatase and rutile, which causes the excited electrons to have a higher reducing power in anatase.

3.2.3. Mechanism of TiO_2 *Based Heterogeneous Photocatalysis*

Semiconductor/electrolyte interfaces have been studied [47-49] from the viewpoint of photoelectrochemical behavior and among them titanium oxides is the one with unique characteristics. The first characteristic is that TiO_2 is chemically stable. It's also electrochemically stable. The second property is that Ti oxide has a low recombination of electron-hole pairs due to low trap number. This property makes TiO_2 to have a high life time of charge carrier. The last property is that TiO_2 can be grown on the substrates in different morphologies. The higher the surface area of the deposited oxide layer, the higher the photocurrent response [47-49].

The reactions during the photocatalysis of TiO_2 are listed below: [57]

1) Charge carrier generation:

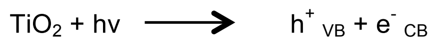

$$TiO_2 + h\nu \longrightarrow h^+_{VB} + e^-_{CB}$$

2) Charge carrier trapping:

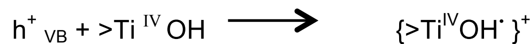

$$h^+_{VB} + {>}Ti^{IV}OH \longrightarrow \{{>}Ti^{IV}OH^{\bullet}\}^+$$

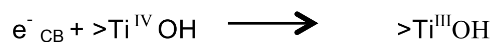

$$e^-_{CB} + {>}Ti^{IV}OH \longrightarrow {>}Ti^{III}OH$$

3) Charge carrier recombination:

$$h^+_{VB} + {>}Ti^{III}OH \longrightarrow {>}Ti^{IV}OH$$

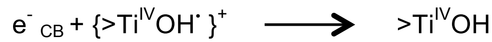

$e^{-}_{CB} + \{>Ti^{IV}OH^{\bullet}\}^{+} \longrightarrow >Ti^{IV}OH$

4) Interfacial charge transfer:

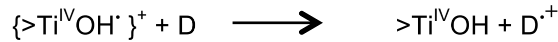

$\{>Ti^{IV}OH^{\bullet}\}^{+} + D \longrightarrow >Ti^{IV}OH + D^{\bullet +}$

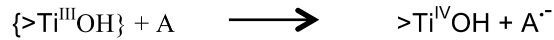

$\{>Ti^{III}OH\} + A \longrightarrow >Ti^{IV}OH + A^{\bullet -}$

$>Ti^{IV}OH$: Primary hydrated surface functionality of TiO_2

$\{>Ti^{IV}OH^{\bullet}\}^{+}$: Surface trapped valance band hole (i.e., surface bound hydroxyl radical)

$\{>Ti^{III}OH\}$: Surface trapped conduction band electron

3.2.4. Photocurrent Measurement Techniques

Several methods have been composed to measure the photocurrent responses such as differential photocurrent spectroscopy, light-spot scanning photocurrent measurement, light beam induced current (LBIC) technique, and also scanning tunneling microscopy to measure spatially resolved primary photocurrents. One of the most popular methods in measuring the photocurrent response of semiconductors is linear sweep photovoltammetry [50-52]. This method involves a supporting electrolyte, such as Na_2SO_4, and photovoltammetry. Photovoltammetry is a voltammetry setup, which contains a slow potential ramp coupled with interrupted illumination of the semiconductor surface [58]. It allows evaluation of both dark electrochemical behavior and also the photoresponse of the film in a single experiment. It is not desirable for the excited electrons to recombine with the generated holes. Therefore, adsorbed water molecules or hydroxyl groups in the supporting electrolyte will be oxidized by holes. The radiation needs to be chopped with a certain frequency as the applied potential is increasing. The result of this method is a photocurrent versus potential curve as shown in Figure 3-10.

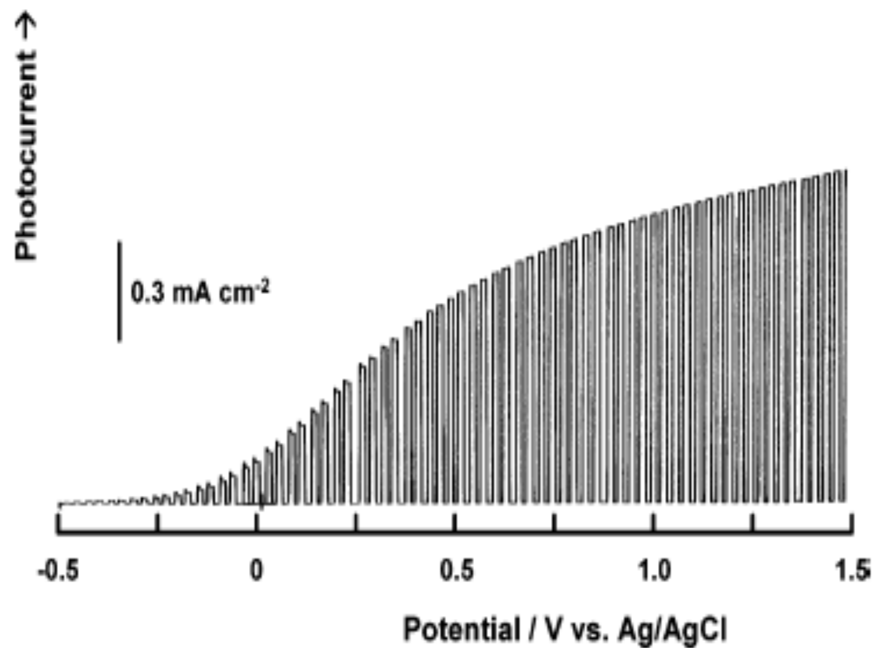

Figure 3-10 Linear sweep photovoltammograms with 0.1 Hz chopped irradiation of a nonporous TiO_2 film obtained by anodization of Ti foil. [59]

In the standard case, the current keeps increasing until it reaches a maximum value, which shows the photocurrent of the semiconductor. There is always a flat area in the beginning of these curves before the electron excitation starts. This flat area is called flat band potential.

The current study explains the effect of morphology of the TiO_2 thin films, created by different methods, on photoelectrochemical responses.

CHAPTER 4

EXPERIMENTAL

4.1 Materials

The current study involves two different sets of experiments. The first part of the research is to develop a TiO_2 thin film on Ti and Al substrate using the PEO method. Aluminum was also considered to be a substrate due to its lower price. Aluminum and titanium samples were finely ground down to 800 grit using SiC paper as the last step. It has been tried to measure the photoelectrochemical response of the developed thin films and examine the effect of the surface morphology on the produced photocurrent. In order to examine the role of morphology, the substrate has been treated or "cleaned" by cathodic EPP prior to the deposition. The cleaning process not only removes the impurities and dirt from the surface, but it also roughens the surface of the substrate. The electrolyte used for the cleaning was 12% $NaHCO_3$ aqueous solution maintained at temperature of 75ºC.

The second experimental part is to deposit TiO_2 thin film on Al and Ti substrates using DC magnetron sputtering technique. One set of Al substrates was used in the sputtering system to be sputter roughened by argon gas, and then, to be coated with titanium dioxide in an argon and oxygen atmosphere using a titanium target. Both EPP-treated (roughened) and mirror finished group of substrates were then coated with TiO_2. A two-inch diameter titanium disk of 99.9% purity was used as the target in sputtering. The atmosphere of the sputtering chamber was a mixture of 2 sccm O_2 (99.99% pure) and 18 sccm Ar (99.99% pure).

Samples are coded as described in Table 4-. Seven types of different samples are being studied.

Table 4-1 Codes of Samples According to Substrates and Method of Coating

Code	Substrate	Coating Method
T	Titanium	PEO
PT	EPP Treated Titanium	PEO
A	Aluminum	PEO
PA	EPP Treated Aluminum	PEO
SPT	EPP Treated Titanium	PVD
SA	Aluminum	PVD
SPA	EPP Treated Aluminum	PVD

4.2 Experimental Setup and Deposition Conditions

4.2.1 Electrolytic Plasma Processing

All processing in the present work was conducted in an electrolytic plasma unit located at CAP Technologies (Baton Rouge, LA), Figure 4- [13]. An experimental laboratory unit was also built in the Surface and Nano Engineering Laboratory at the University of Texas at Arlington, Figure 4-2. This processing equipment uses “foam” technology, meaning that the work piece is surrounded by foam rather than by a thin layer of electrolyte or being immersed into the electrolyte.

The active elements of the EPP are the anode and the cathode (work piece). As illustrated in Figure 4-, there should be a flow from anode to the cathode surface in order for the whole system to remain conductive. EPP does require a specific uniform plasma state. The distance between the anode and the cathode is one of the parameters that need to be adjusted accordingly to obtain a stable plasma. This distance can be changed by changing the anode position. The electrolyte is being pumped directly from the supply tank to the vertical cylinder, which is placed above the anode disk. The flow rate of the electrolyte can also be adjusted by the pump and also size of the holes of the anode. A heater is also provided in order for the

electrolyte to stay at the required temperature. The power is provided by a DC power supply. The cathode should be connected to the power supply and anode goes to the ground.

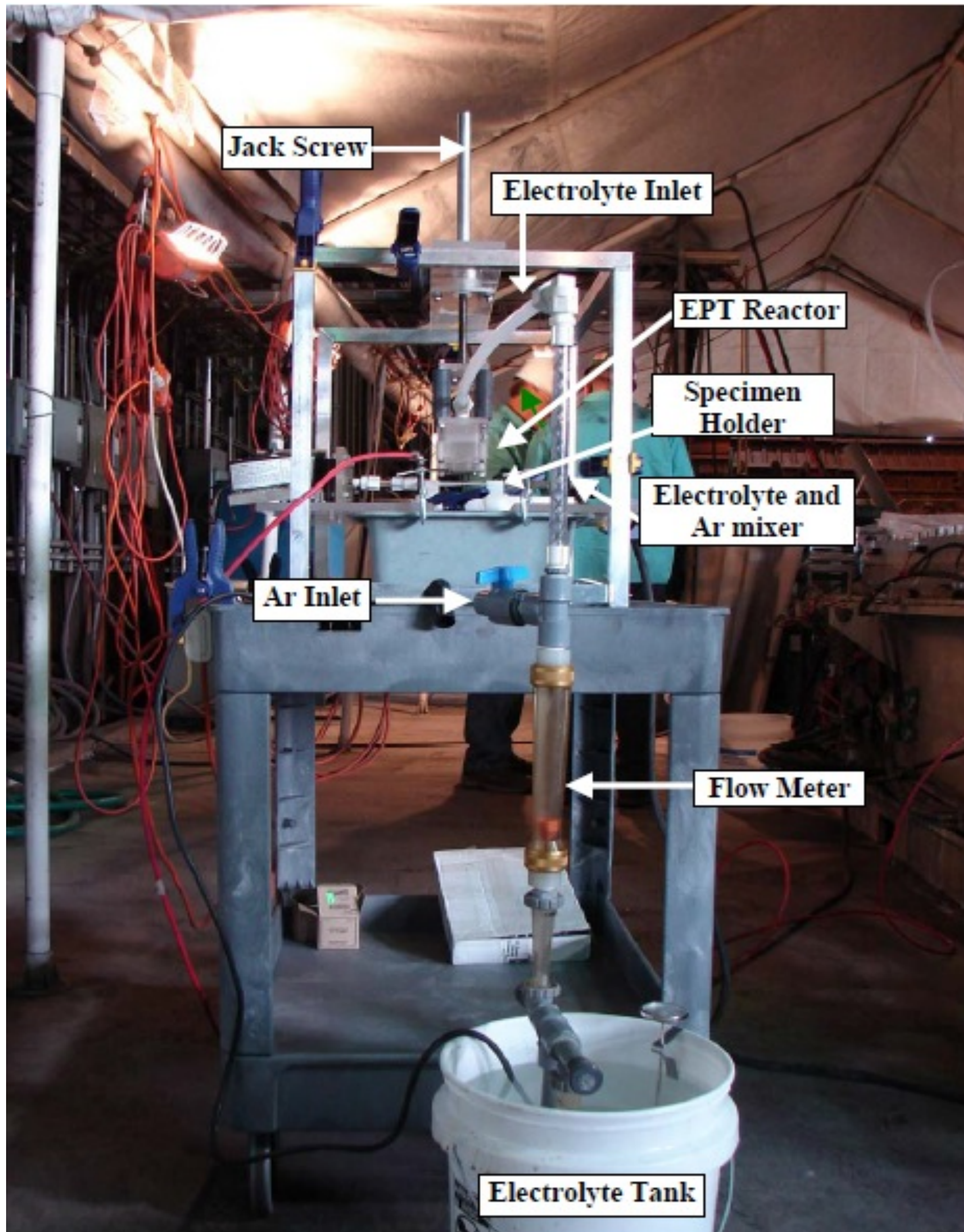

Figure 4-1 CAP Technologies EPP reactor that was designed to handle different types of specimens. [13]

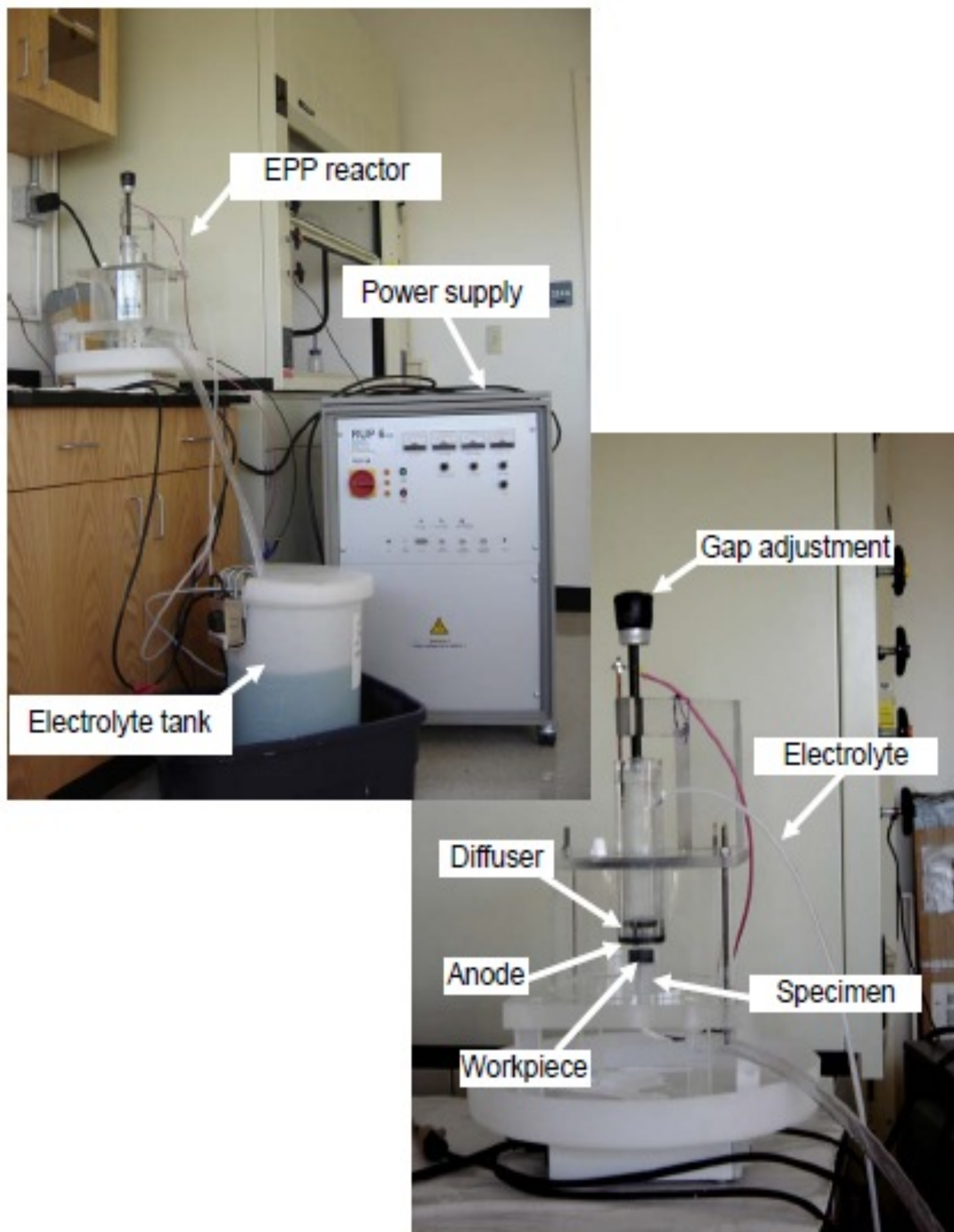

Figure 4-2 EPP reactor and setup built at UTA; right side image represents the close up view of the reactor. [13]

The electrolyte used for the cleaning process was 12% $NaHCO_3$ aqueous solution that had to stay at 75ºC in order for the baking soda to get dissolved. The cleaning process required an applied voltage of 140 V and the current was 11-14 A. The process was performed for 10, 20, and 30 s while the electrode gap was fixed at ~5 mm. All three substrates (Al and Ti) were cleaned with the same procedure.

For the next step, TiO_2 was deposited on aluminum and titanium substrates by aqueous plasma electrolyte deposition method, which is the same as plasma electrolytic oxidation with anodic polarization. The applied voltage during the process was 250 V for Ti and 450 V for Al substrate. Both flat and mirror finished substrates were deposited by this method in order to be able to examine the effect of surface morphology on photoelectrochemical response of TiO_2 film.

4.2.2 DC/RF Magnetron Sputtering

TiO_2 was also deposited by DC magnetron sputtering on aluminum and titanium substrates. Figure 4-3 presents a schematic of the sputtering system. The stainless steel chamber has a cylindrical shape and is equipped with two magnetron guns (2 inches diameter) with both DC and RF biasing capability. Chamber vacuum is accomplished down to 25 mtorr by a Trivac 30A mechanical pump, and beyond that vacuum is achieved by an Ebara FS 8 series cryopump and compressor with a base vacuum level of 1×10^{-6} Torr. Figure 4-4 shows the picture of the sputtering system at UT Arlington, which has been used for the current study.

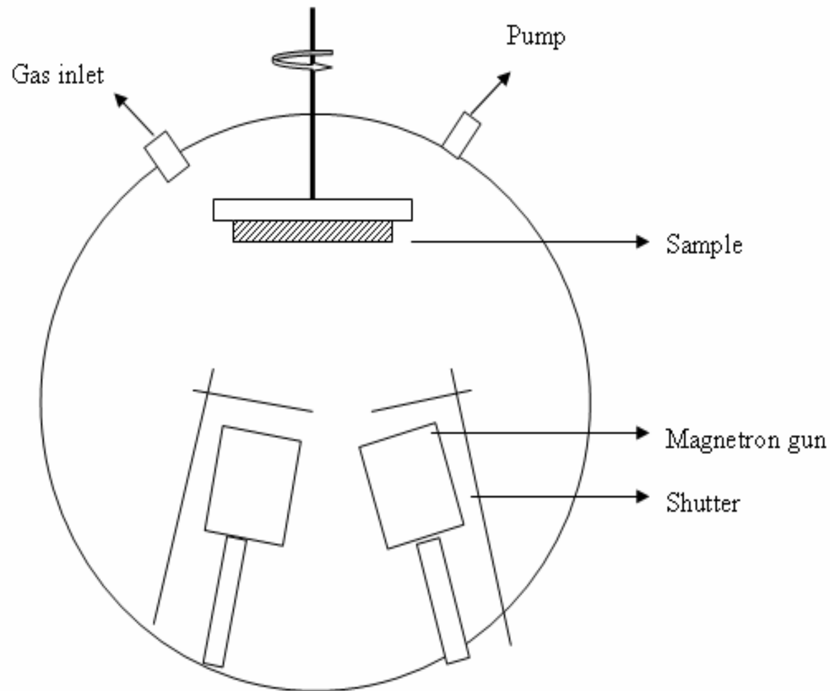

Figure 4-3 Schematic representation of the home built hybrid plasma CVD and PVD system. [60]

Titanium dioxide thin film was also created by DC magnetron sputtering without any external substrate heating. A glassman high voltage inc. (series EK) power supply was used for this experiment. The distance between the gun and the substrates was set to be about 90 mm. Titanium target of 99.99% purity with 2-inch diameter was used as the cathode. A base pumping system was used to achieve a base pressure bellow 1×10^{-6} Torr. High purity Ar (99.99%) and O_2 (99.95%) were used as the sputtering and reactive gases (18 sccm Ar and 2 sccm O_2).

The sputtering procedure includes three deferent steps. Prior to the main deposition, the substrates where first sputter roughened by Ar^+ for 30 min. Sputter roughening helps to clean the surface of the substrate from some impurities and it also helps to create some features on the surface of the substrate in order to increase the roughness of the surface, which is favorable in order to get a higher surface area and higher photocurrent. Roughening was

conducted at 15 mTorr of pressure with Ar gas as the sputtering gas and an applied DC voltage of -1000. Right after roughening, the bias voltage was decreased to -500 and Ti was deposited on the substrate for 5 min. For Ti deposition, Ar gas was introduced to the system by flow rate of 18 sccm. Again, the total pressure of the chamber was set at 15 mTorr and power of 200 W was applied to the Ti target for deposition. After 5 min of Ti deposition, 2 sccm of O_2 is also introduced to the chamber in order to have titanium dioxide deposition. The layer of Ti was deposited prior to oxygen entering the system to prevent oxidation of the Al substrate. TiO_2 deposition took place for 1 h. After completing the depositions, the O_2 was cut off and the chamber was filled with Ar to maintain at inert environment. Subsequently, the chamber was vented and opened to room air.

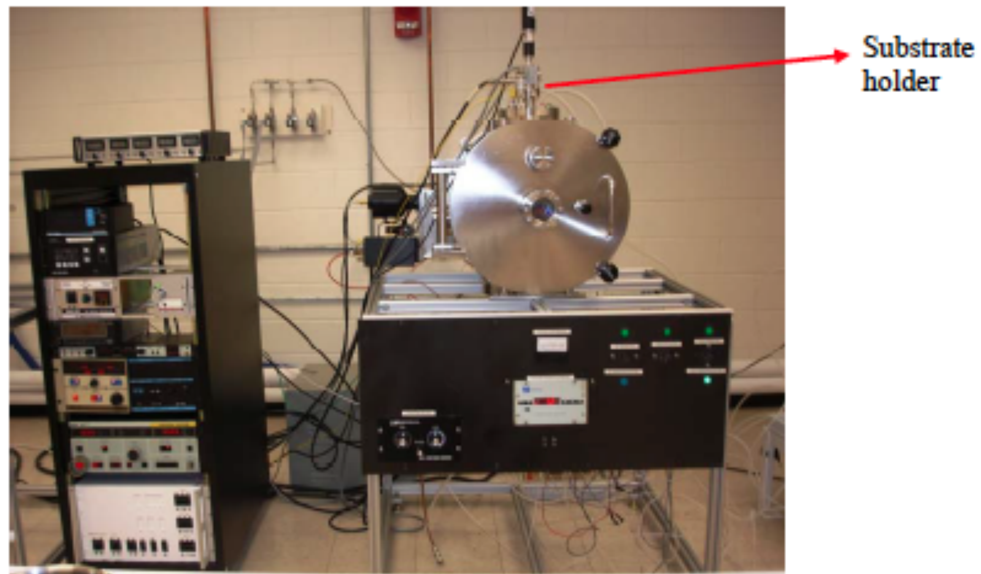

(a)

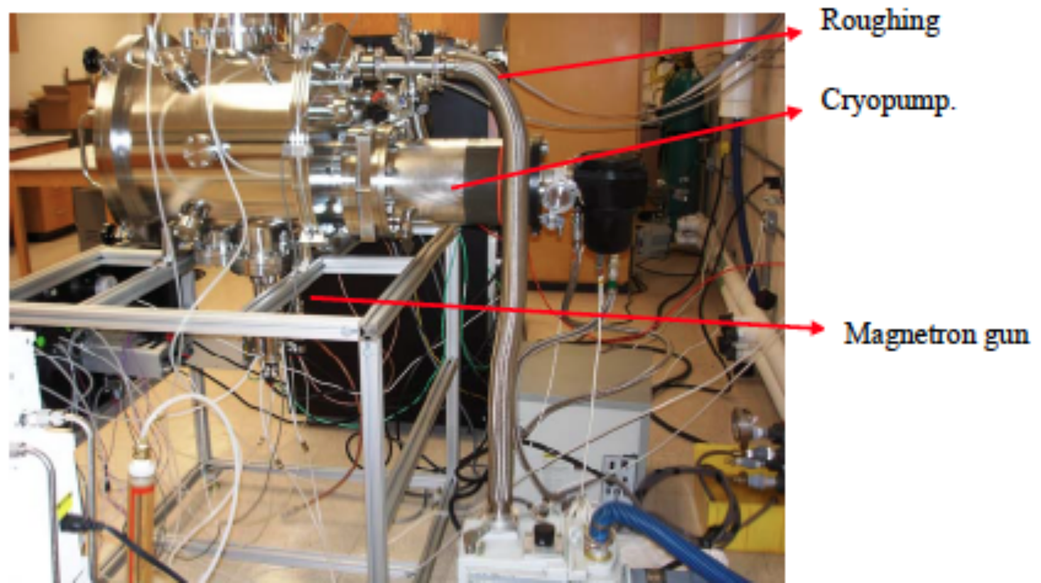

(b)

Figure 4-4 Hybrid plasma CVD and PVD system (a) Front view of the system, (b) Side view of the system. [60]

4.3 Characterization of Produced Materials

Several techniques were employed to characterize the TiO_2 coated specimens.

4.3.1 Photocurrent Measurement

Photoelectrochemical measurements were done by a standard three-compartment, three-electrode electrochemical cell. The cell setup basically includes A large Pt coil and an Ag|AgC. KCl reference electrode (Microelectrode Inc., NH), along with the working electrode. The UV light source was a 150 W xenon arc lamp (Oriel, Stratford, CT), which produces the nominal incident photon flux of 0.59 mW/cm^2 at 340 nm with a bandwidth of 4 nm. All the reported potentials during the experiments are quoted with respect to the reference electrode. Monochromatically measurement was conducted on photon flux by an Oriel model 70260 Radiant Power/Energy meter. The distance between the working electrode and the radiation source was set to be 8 cm. Photovoltammetry profiles were recorded on a model CV-27 Voltammograph (Bioanalytical Systems, West Lafayette, IN) equipped with a model VP-6414S Soltec X-Y recorder. The electrolyte used for these measurements was aqueous 0.5 M Na_2SO_4 solution. The photovoltammogram scans were obtained using a slow potential sweep (2 mV/s) in conjunction with interrupted irradiation (0.1 Hz) of the semiconductor film. All the following measurements were performed at laboratory ambient temperature (~25 °C).

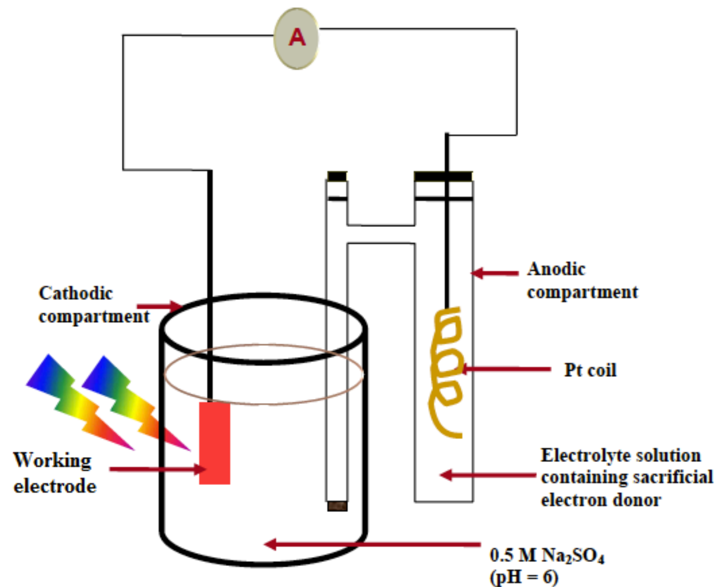

Figure 4-5 Schematic principal of photoelectrocurrent measurement by linear-sweep voltammetry.

4.3.2. Surface Morphology and Roughness Measurement

Surface properties, such as surface roughness, skewness, flatness, etc., can be achieved using optical interference profilometry [61]. Profilometry is a fast and nondestructive method for surface characterization. A WykoNT9100 instrument was used in the present work. R_a reports the average surface roughness, which is measured in two-dimensional measurement. This is why surfaces with similar average surface roughness values (R_a) sometimes actually have vastly different surface topographies.

The other method used for observing surface properties is 3D surface metrology uses 3D surface profilers to provide non-contact measurement of surface features. This technique includes white light based interferometric microscopes (optical profilers) and 3D confocal microscopes. It is a non-contact and non-destructive method, providing effective and repeatable imaging and measurements.

4.3.3. Scanning Electron Microscopy (SEM)

Surface morphology analysis of the processed materials is conducted by SEM. Surface features and their shape, size, and distributions are being examined by SEM. These features indicate how processing was dynamically interacting with the surface. Other observations such as thickness of the coatings, interface, and porosity can be examined by cross section SEM. Epoxy mounted samples were in contact with carbon tape in order to avoid charging. Energy-dispersive X-ray spectroscopy (EDS) was also employed to evaluate the elemental composition of the layers and coatings.

4.3.4. X-ray Diffraction

The phase structures of the created thin films were analyzed by x-ray diffraction (XRD) using a Siemens D500 x-ray diffractometer operated in the Bragg-Brentano mode. A Cu K_α radiation source (λ_{Cu} = 0.154 nm), with accelerating voltage and filament current of 40 kV and 30 mA, were be used to perform detector axis scan mode. The peaks were then identified using database search application (Jade platform).

4.3.5. Transmission Electron Microscopy (TEM)

More detailed observations of the microstructure of the thin films were performed using high resolution (HR) TEM (model: Hitachi H-9500 microscope) coupled with Fast Fourier Transformation (FFT). HRTEM is a valuable tool for the phase identification of the coating. Using TEM at an accelerating voltage of 300 kV with a lattice resolution of 0.18 nm, high-resolution lattice images of crystalline nanoparticles were acquired.

TEM samples were prepared using the same sputtering condition. Deposition time was decreased to 5 minutes, in order to obtain a very thin film through which the HRTEM electron beam can penetrate. The TiO_2 film was deposited directly onto a carbon coated copper grid with 300 mesh, allowing for a convenient way to quickly view the microstructure of the films using TEM.

4.3.6. Raman Spectroscopy

The Raman spectrometer used for the study was a Thermo scientific DXR spectrometer using diode pumped solid-state type laser as a source of illumination. To record the Raman spectra a solid-state laser was used with a frequency of 532 nm with maximum power output of 10 mW. Raman spectroscopy was performed on the samples in order to characterize the phase of the created thin films

CHAPTER 5

RESULTS AND DISCUSSION

5.1 EPP Surface Patterning

Surface morphology characterization of EPP treated materials was conducted using SEM and profilometry.

5.1.1. SEM

For SEM analysis, the acceleration voltage was set in the range of 10-25 keV in order to acquire the top-view micrograph. The micrograph of the surface of EPP treated Al and Ti substrates are respectively shown in Figure 5-1 and Figure 5-2. According to the following micrographs, a progressive development of randomly distributed hills and valleys are observed as the processing time increases. As previously discussed in the literature, the formation of this morphology is due to occurring of continuous plasma, melting and solidification of the surface. It can also be observed from the micrographs that as the plasma time increases, the morphology of the surface turns more “tortuous”, which can be due to the relatively low melting temperature of Al and Ti. [13]

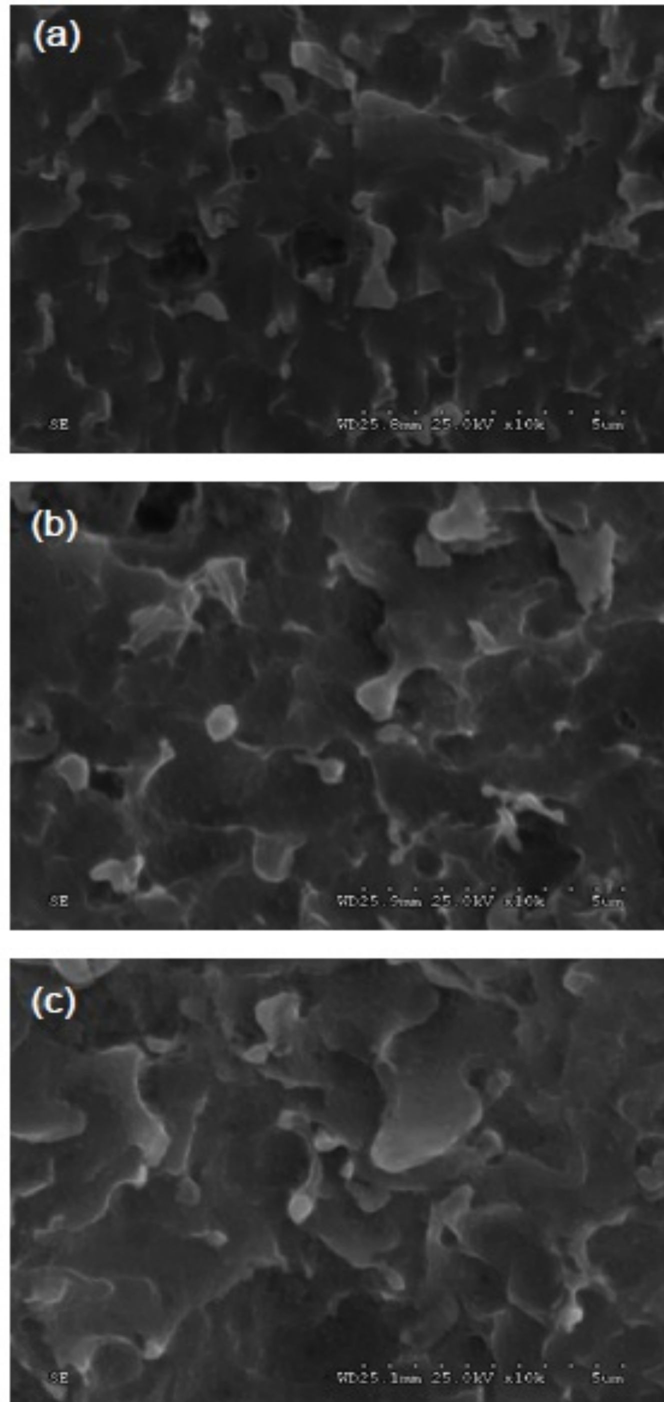

Figure 5-1 Top surface SEM micrographs of EPP-treated 1100 Al at different processing times of (a) 10 s (b) 20 s, and (c) 30 s. [13]

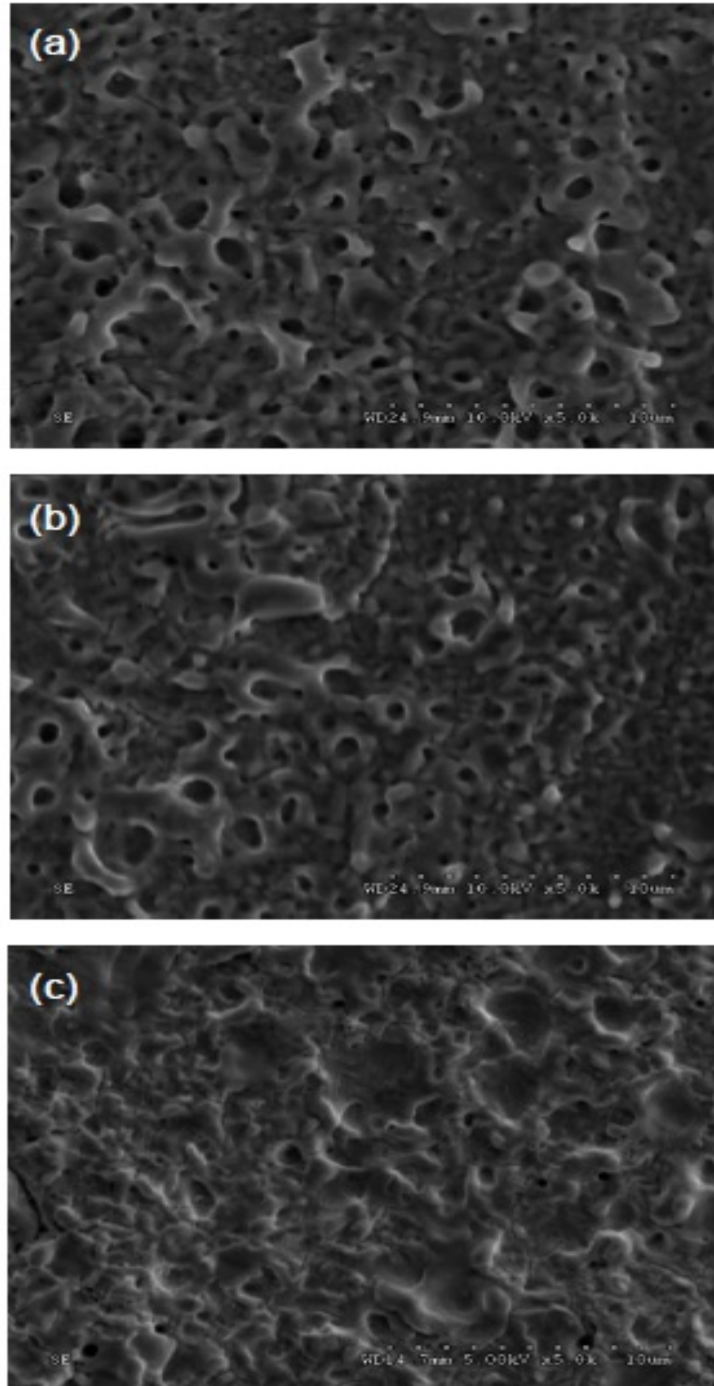

Figure 5-2 Top surface SEM micrographs of EPP-treated pure Ti at different processing times of (a) 10 s (b) 20 s, and (c) 30 s. [13]

5.1.2 Profilometry

Optical profilometer was used in order to study the effect of processing time on the topology of the surface. The main parameter to characterize overall morphology of the surface is R_a, which represents the roughness average, the arithmetic mean of the absolute values of the surface departures from the mean plane [13]. Figure 5-3 shows the variation of R_a with processing time. As illustrated, the surface roughness generally decreases as the duration of plasma increases.

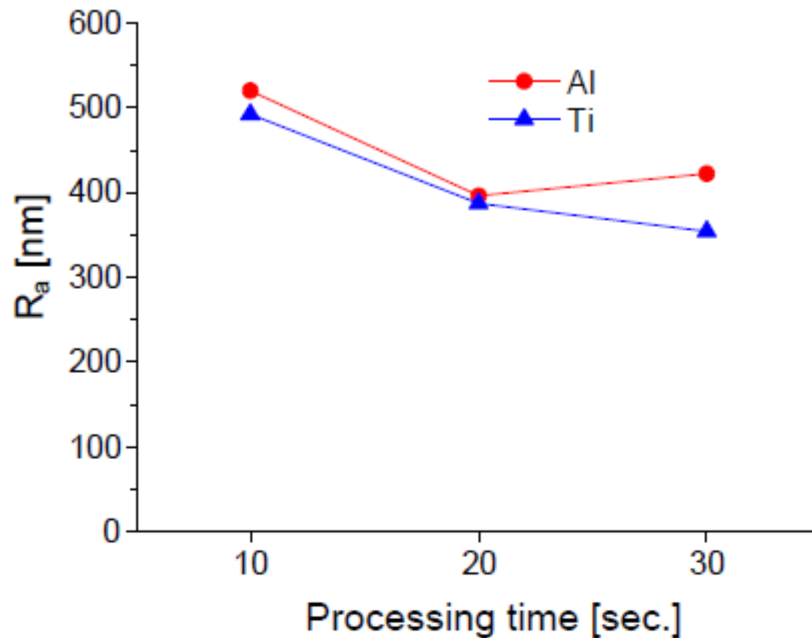

Figure 5-3 R_a as a function of processing time. [13]

5.2 PEO Coatings

EPP treated (roughened) and mirror finished Al and Ti substrate were coated by TiO_2 thin film with aqueous plasma electrolyte deposition method, which is the same as plasma electrolytic oxidation with anodic polarization. The thickness of the film is reported to be around 4-6 μm thick on Ti substrates and 7-10 μm thick on Al. SEM and profilometry observations has

been used to determine the morphology of the deposited film. The phase of TiO_2 deposited film was identified by means of low angle XRD. The results have also been confirmed, using Raman. The photoelectrochemical response of the deposited thin film was measured and the effect of morphology has been examined by photocurrent measurements.

5.2.1. Photoelectrocurrent Measurement

Photoelectrocurrent measurement was conducted on all four samples (A, PA, T, and PT). A standard single-compartment, three-electrode electrochemical cell was used with Ag|AgCl|satd. KCl reference electrode (Microelectrode Inc., NH), along with the working electrode.

Figure 5-4 shows the photoelectrochemical behavior of T and PT samples. As expected, the photocurrent produced by PT is higher than that of T, meaning that as the roughness of the film increases, the produced current increases as well.

No photocurrent could be detected for Al substrate samples, which were coated by TiO_2. It has been justified by knowing that Al substrate oxidized during PEO. This undesirable oxidation causes the formation of Al_2O_3 on the surface as a barrier and the thin film produces no photocurrent.

Since no photocurrent was obtained from the Al substrates, the rest of characterizations have mainly been done on the samples with Ti substrate. There are also selective analyses done on Al substrates as well.

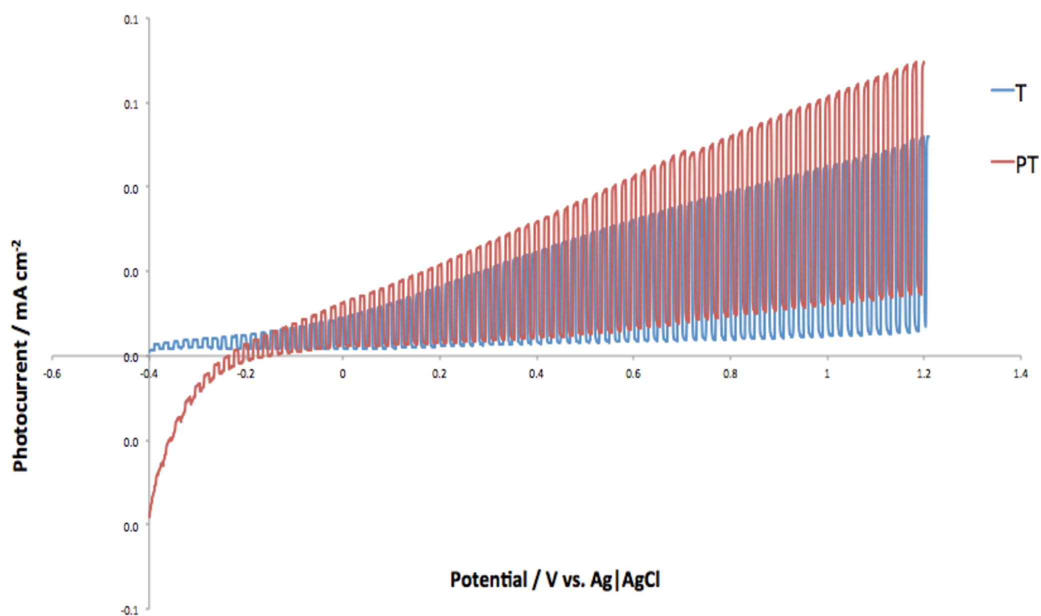

Figure 5-4 Photoelectrocurrent activity of T (flat Ti substrate coated with TiO_2) and PT (EPP cleaned Ti substrate coated with TiO_2).

5.2.2 X-ray Diffractometry

The phase structure of the deposited thin films on both Al and Ti substrates was checked by Siemens D-500 X-ray diffractometer with CuKα radiation source. Low angle analysis was conducted in order to get the phase structure of the film, not the substrates.

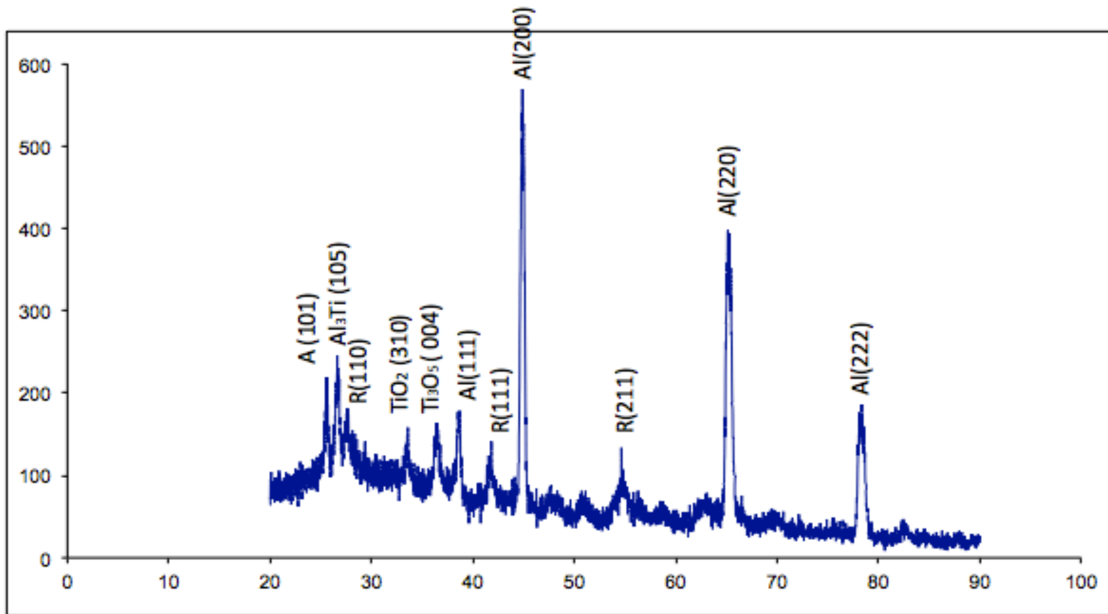

Figure 5-5 XRD pattern of A (Flat Al substrate coated by TiO_2).

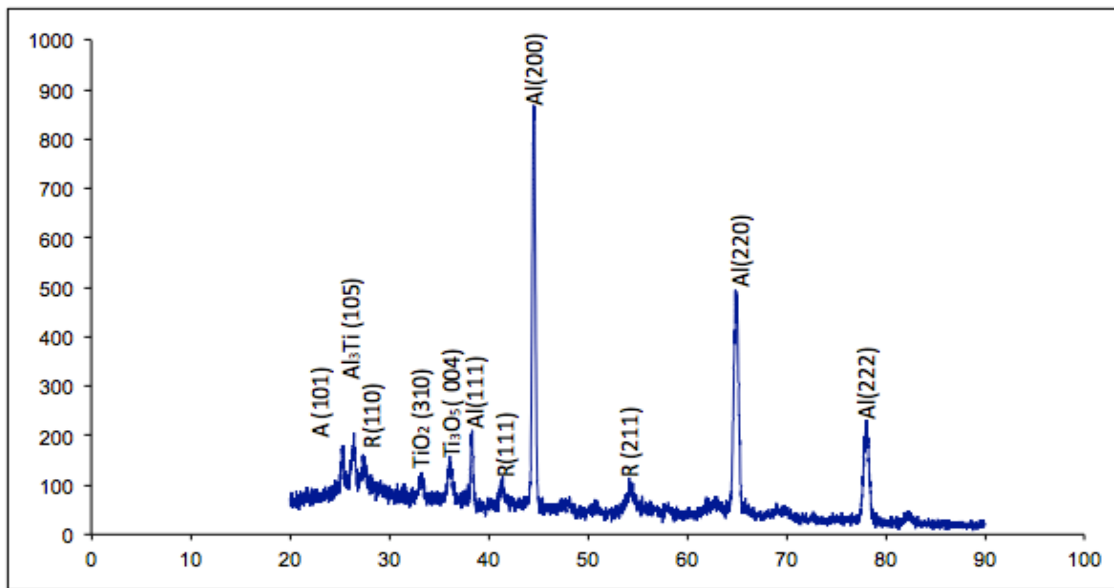

Figure 5-6 XRD pattern of PA (EPP treated Al substrate coated by TiO_2).

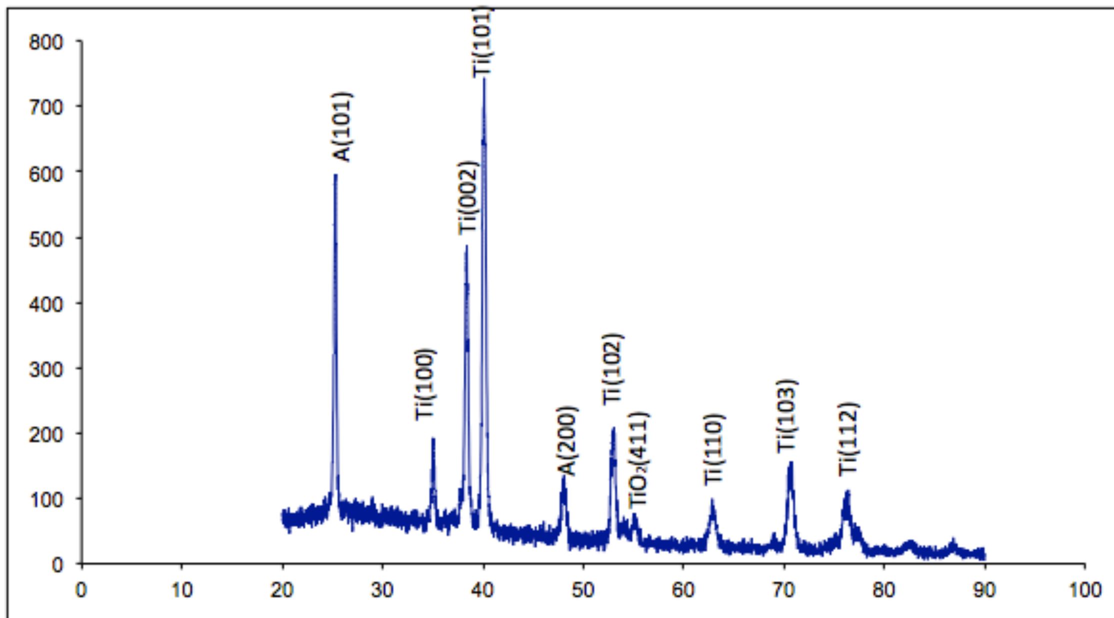

Figure 5-7 XRD pattern of T (Flat Ti substrate coated by TiO_2).

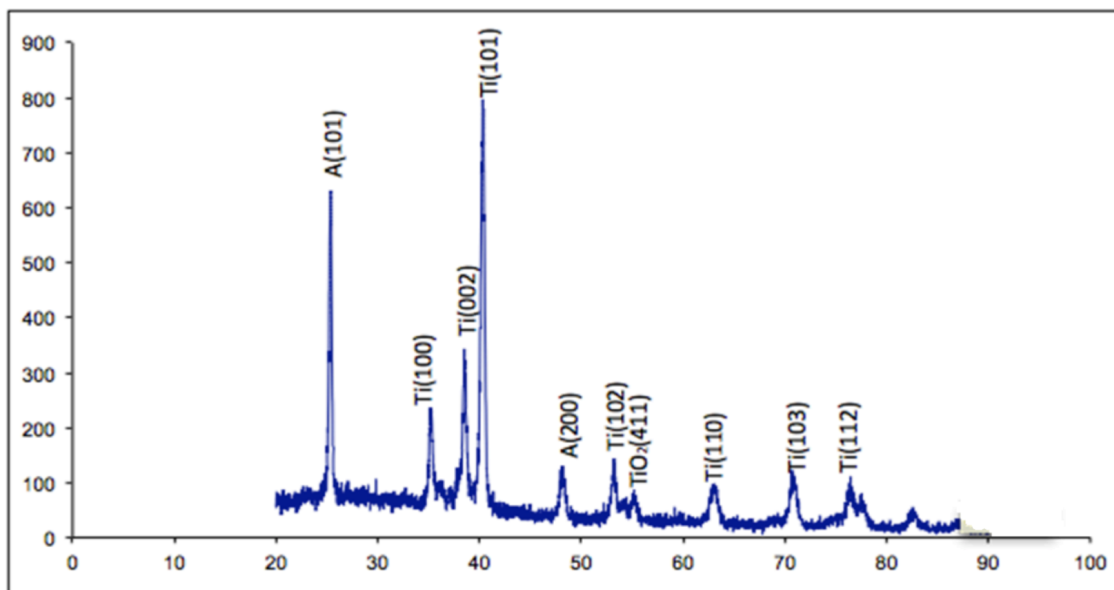

Figure 5-8 XRD pattern of PT (EPP treated Ti substrate coated by TiO_2).

As it can be observed in the XRD patterns, the TiO_2 thin film is crystalline in Anatase form on Ti substrate and it is almost amorphous on Al substrates. The type and crystallinity of

the thin film has not changed by changing the morphology of the substrate. Several peaks for different types of titanium oxide also exist on the XRD pattern of A and PA sample; however, the peaks are not intense enough and we consider the thin film to grow amorphous on Al substrates.

The grain size (*d*) of the deposited thin film can be calculated using Scherer equation [62]: $d = \frac{0.9\lambda}{B\cos\theta}$, where *B* is the full width at half maximum (FWHM) of the diffraction peak, and θ is half of the diffraction angle. λ is the wavelength of the x-ray source, which is 1.54×10^{-10} Å. Therefore, the approximate grain size of the anatase thin film, deposited on Ti substrate is calculated to be about 62 nm.

5.2.3. SEM

The morphology of the surfaces of coated samples has been investigated by SEM. In order to be able to get good micrographs of the samples surfaces, they need to be coated by a conductive material. A sputtering system (model type: *Torr International Inc. CrC-100*) was used for this coating. Silver sputtering was done on the sample surfaces for 2 min, using a silver target.

It can be seen that the microstructure is composed of a random distribution of hills and valleys. Comparing the morphologies of T and PT in different magnifications confirms the fact that roughness of the surface increases by prior EPP cleaning. This is also the reason why the photoelectrocurrent produced by PT is higher in comparison to T.

Figure 5-12 represents the microstructure of EPP treated Al substrate coated with TiO_2 (PA). It can be observed that the microstructure is again composed of many features, giving the surface a high roughness.

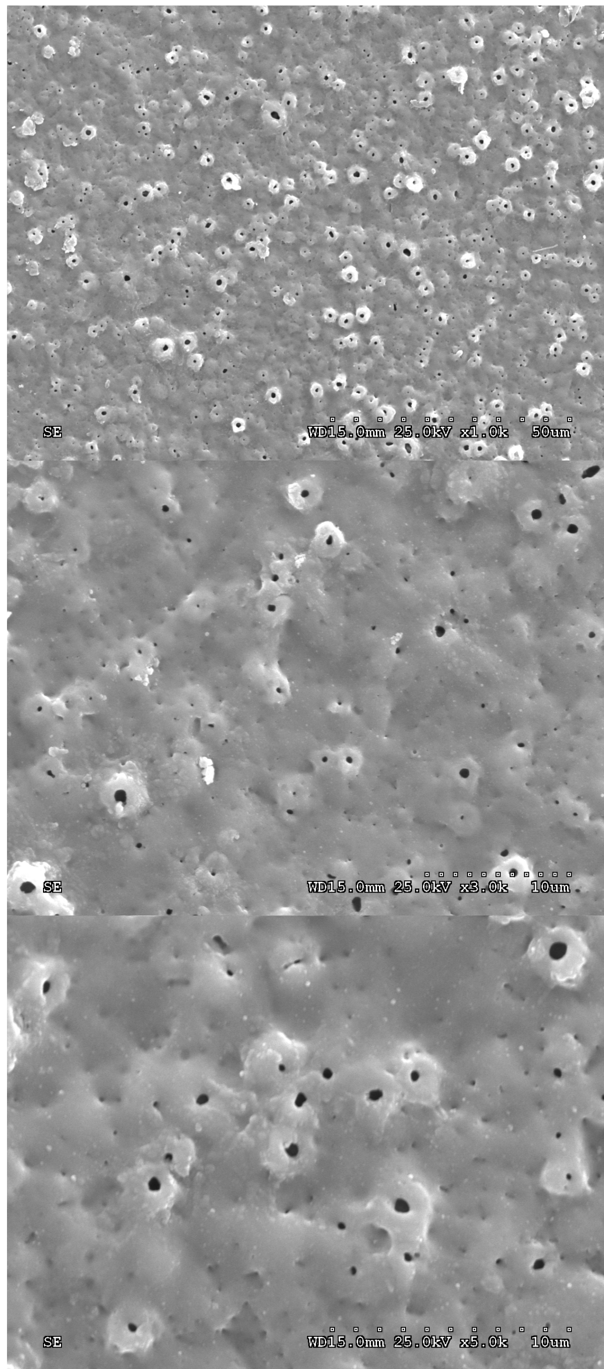

Figure 5-9 The microstructure of flat Ti substrate coated with TiO_2 (T) at different magnifications.

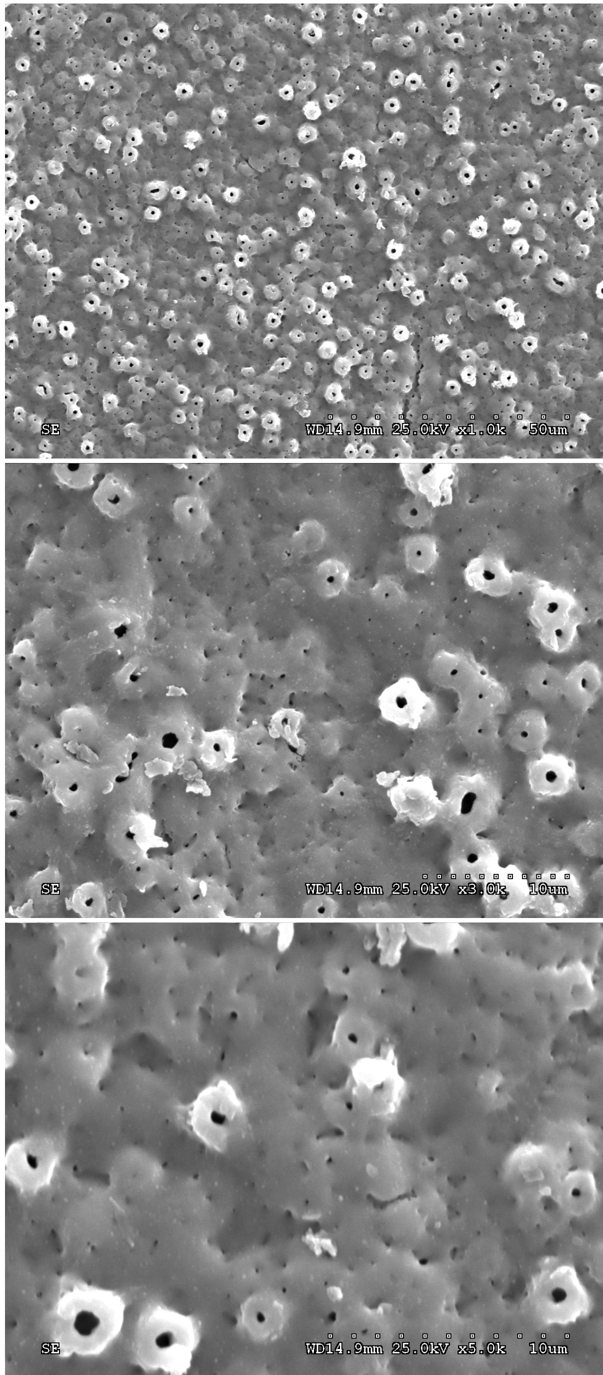

Figure 5-10 The microstructure of EPP treated Ti substrate coated with TiO_2 (PT) at different magnifications.

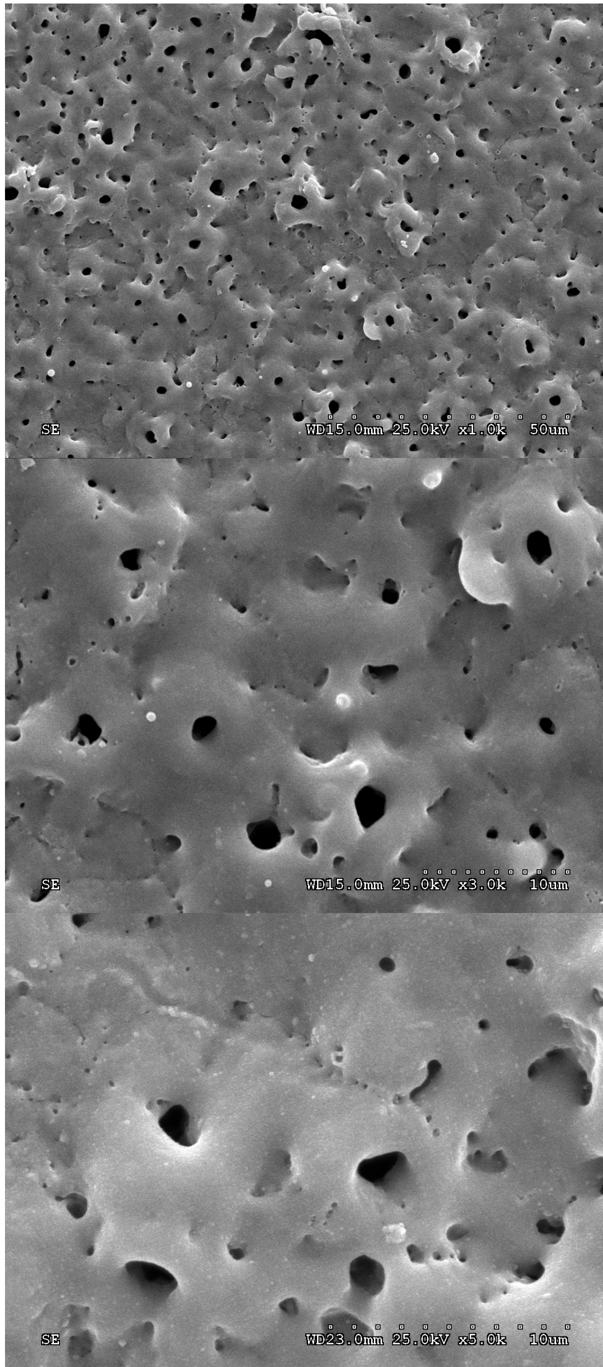

Figure 5-11 The microstructure of flat Al substrate coated with TiO_2 (A) at different magnifications.

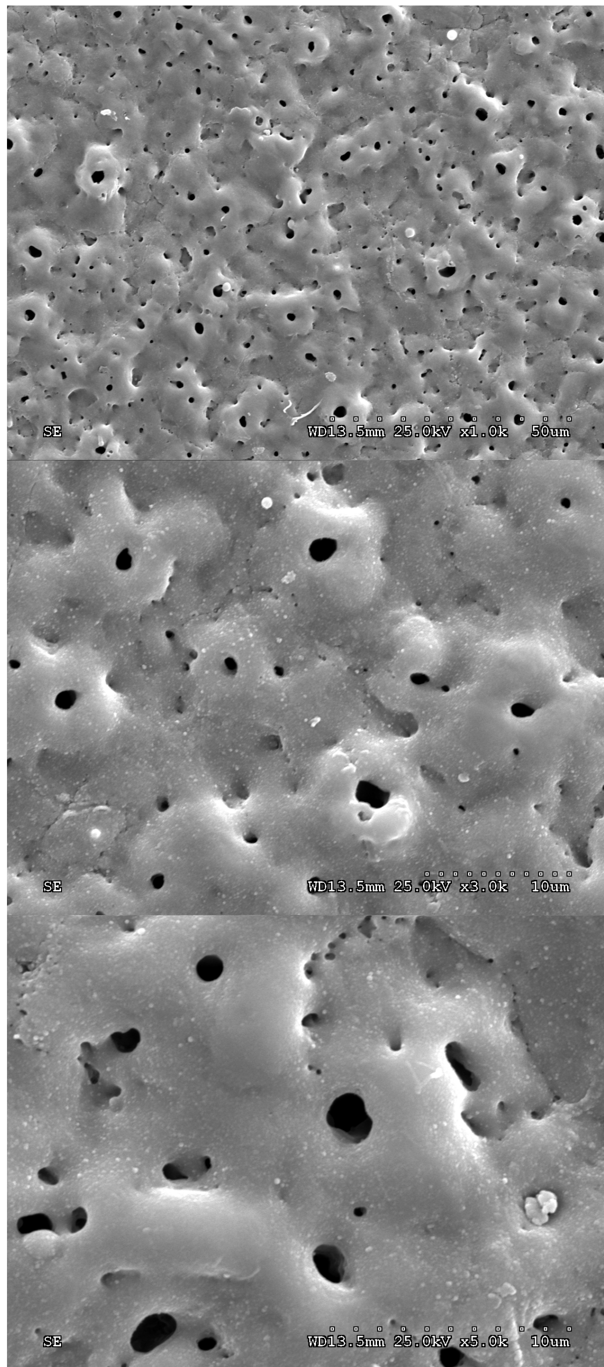

Figure 5-12 The microstructure of EPP treated Al substrate coated with TiO_2 (PA) at different magnifications.

5.2.4. Profilometry and Roughness Measurement

The average roughness of all samples was measured by profilometer. The three dimensional topography of the surface was also studied. As reported in Figure 5-13, it has been discovered that for the Ti substrates, the roughness of the surface increases after coating by TiO_2. On the other hand, for aluminum substrates, the roughness remains constant after coating with TiO_2.

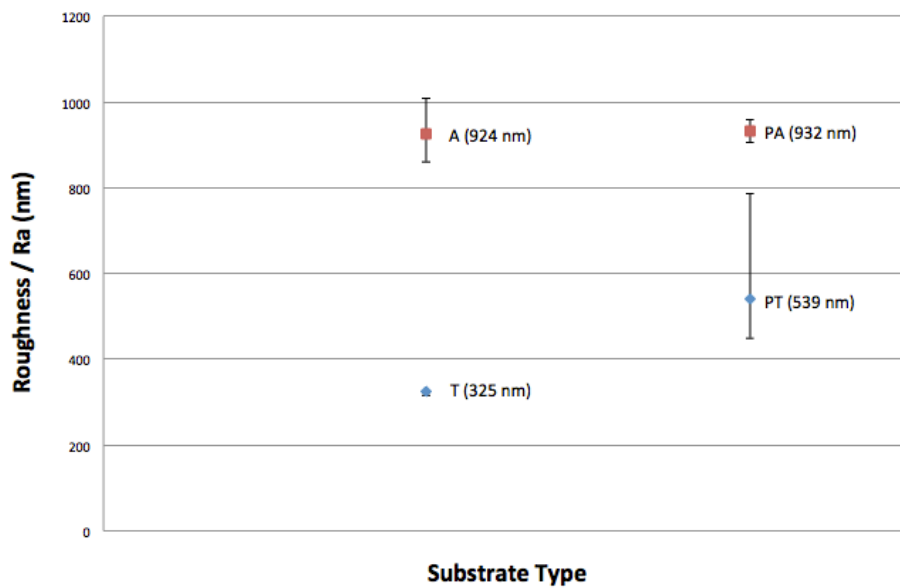

Figure 5-13 Average roughness of TiO_2 thin film on flat and EPP treated samples.

As it was expected, the roughness of the deposited thin films follows the roughness of the substrate. In other words, the film has a higher roughness when deposited on the prior EPP patterned substrate.

Figure 5-14 and Figure 5-15 show the three-dimensional topography of surfaces of samples (T, PT, A and PA). The roughness of the surfaces is also displayed in the images. Also, two-dimensional topographies of the samples are shown in Figure 5-16 to Figure 5-19.

As illustrated in 2D and 3D topologies of the surfaces, all of the coated samples have rough surfaces with valleys and hills. This special topography is due to the EPP method used

for coating the substrates. As discussed before, the EPP coating is the result of the high voltage on the substrate surface and continuous break down and solidification of the film and also the substrate. This is the reason why such features are found on the surface of the samples.

Surface Stats:

Ra: 1.07 um

Rq: 1.33 um

Rt: 16.41 um

Measurement Info:

Magnification: 5.00

Measurement Mode: VSI

Sampling: 1.98 um

Array Size: 640 X 480

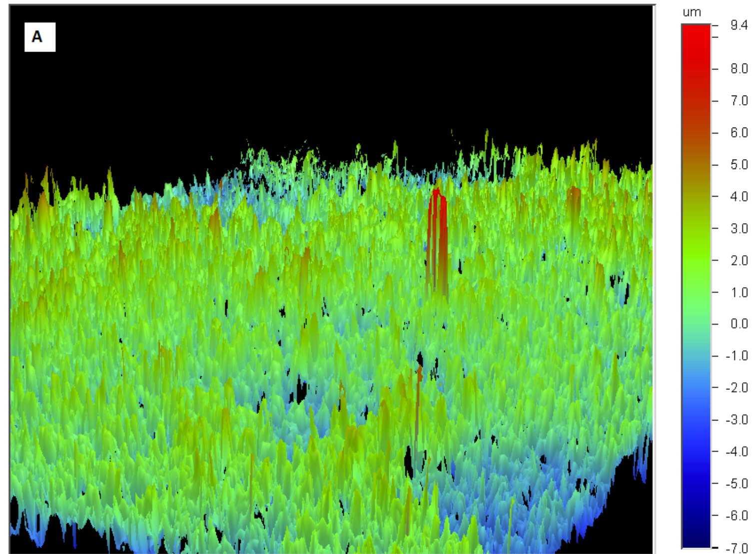

Surface Stats:

Ra: 912.88 nm

Rq: 1.15 um

Rt: 14.47 um

Measurement Info:

Magnification: 5.00

Measurement Mode: VSI

Sampling: 1.98 um

Array Size: 640 X 480

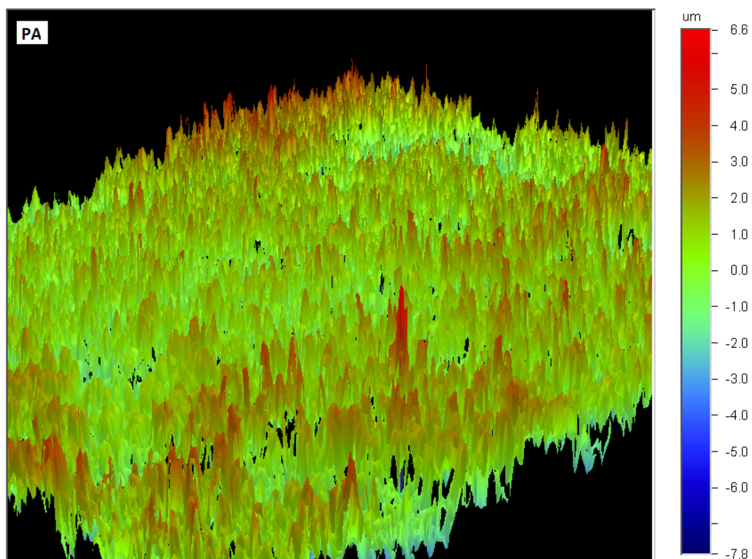

Figure 5-14 Three-dimensional topography of TiO_2 thin film on flat and EPP treated Al substrates.

Surface Stats:

Ra: 316.11 nm

Rq: 401.85 nm

Rt: 5.11 um

Measurement Info:

Magnification: 5.00

Measurement Mode: VSI

Sampling: 1.98 um

Array Size: 640 X 480

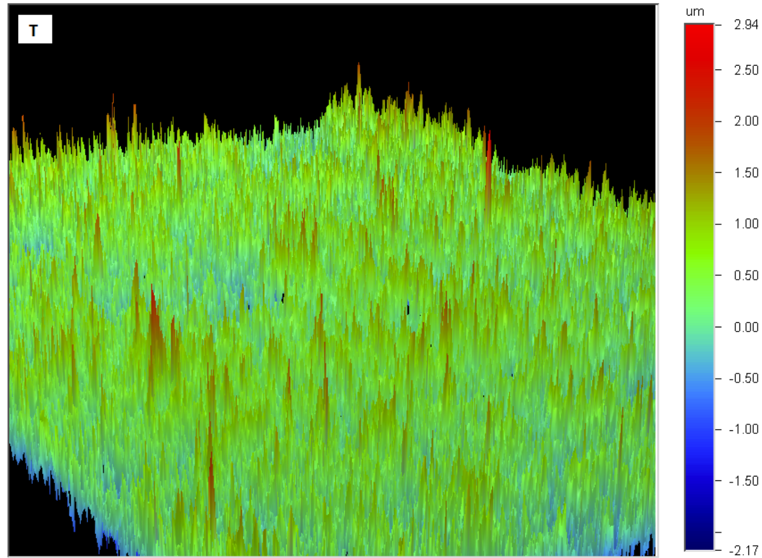

Surface Stats:

Ra: 449.07 nm

Rq: 576.56 nm

Rt: 7.23 um

Measurement Info:

Magnification: 5.00

Measurement Mode: VSI

Sampling: 1.98 um

Array Size: 640 X 480

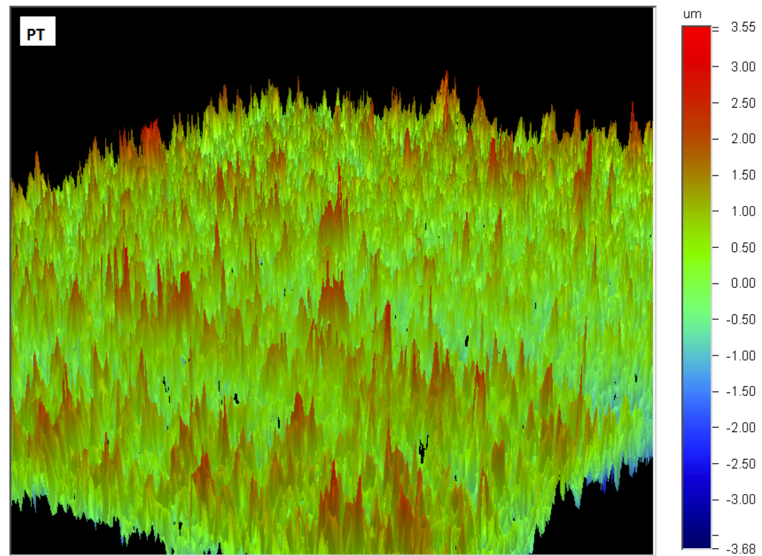

Figure 5-15 Three-dimensional topography of TiO_2 thin film on flat and EPP treated Ti substrates.

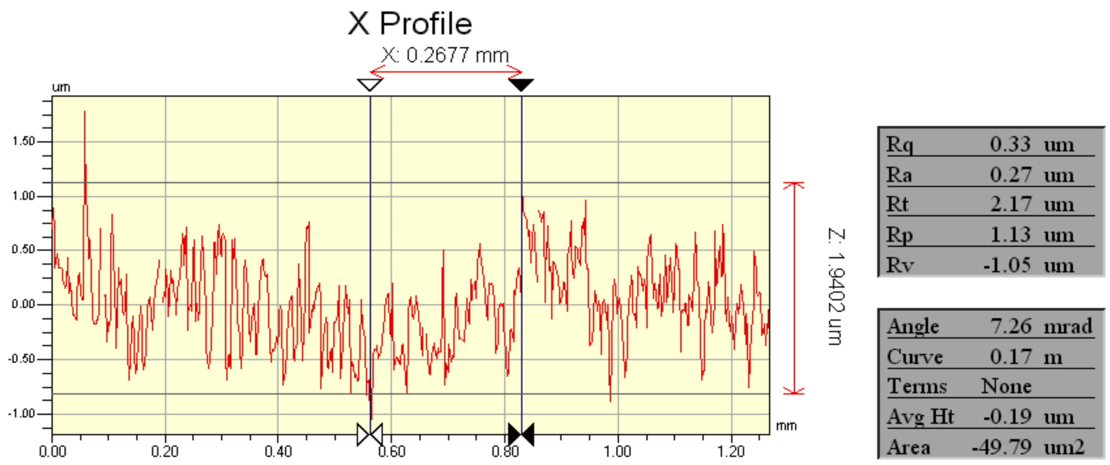

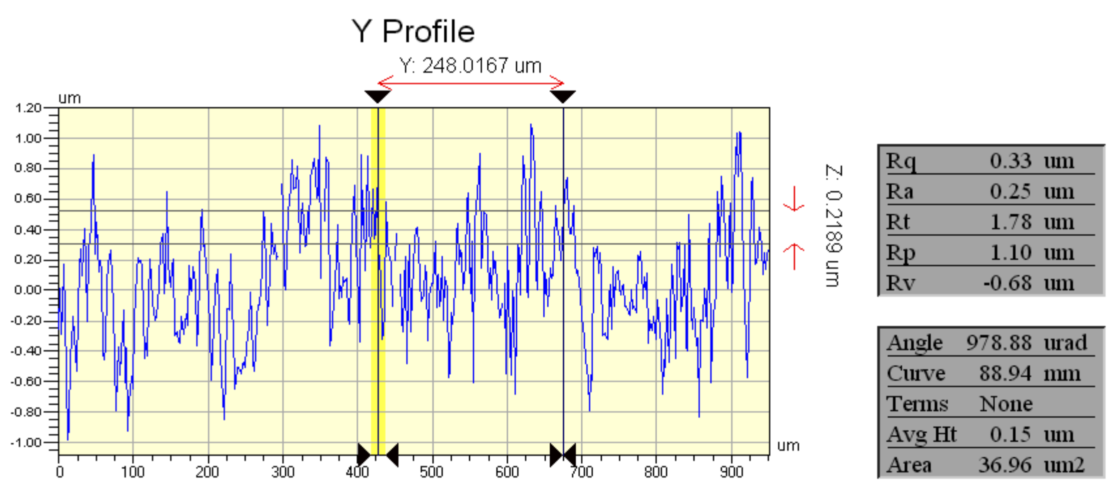

Figure 5-16 Two-dimensional topography of the surface of T.

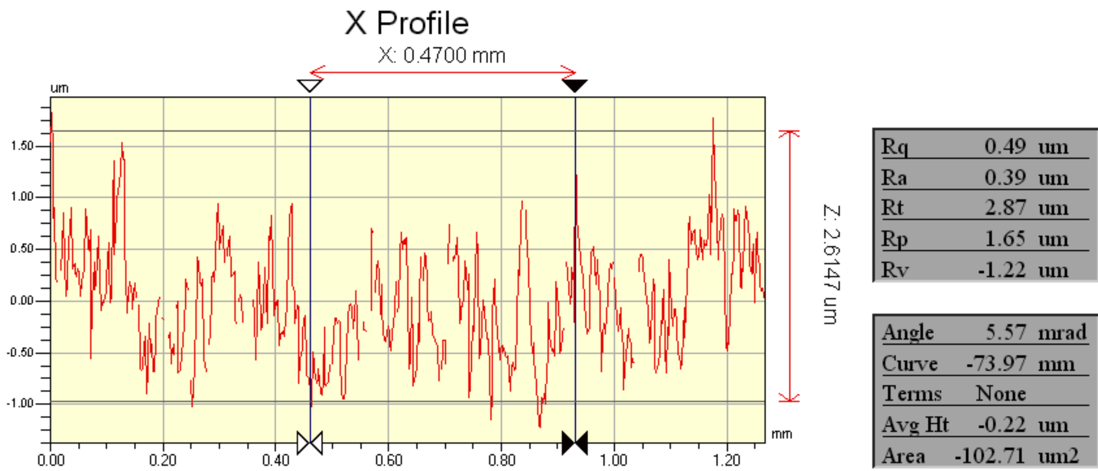

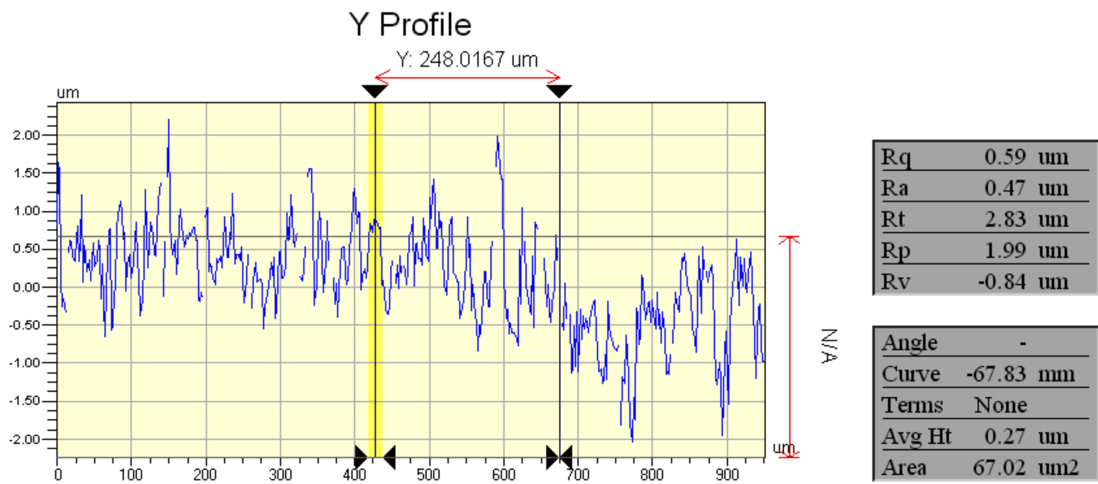

Figure 5-17 Two-dimensional topography of the surface of PT.

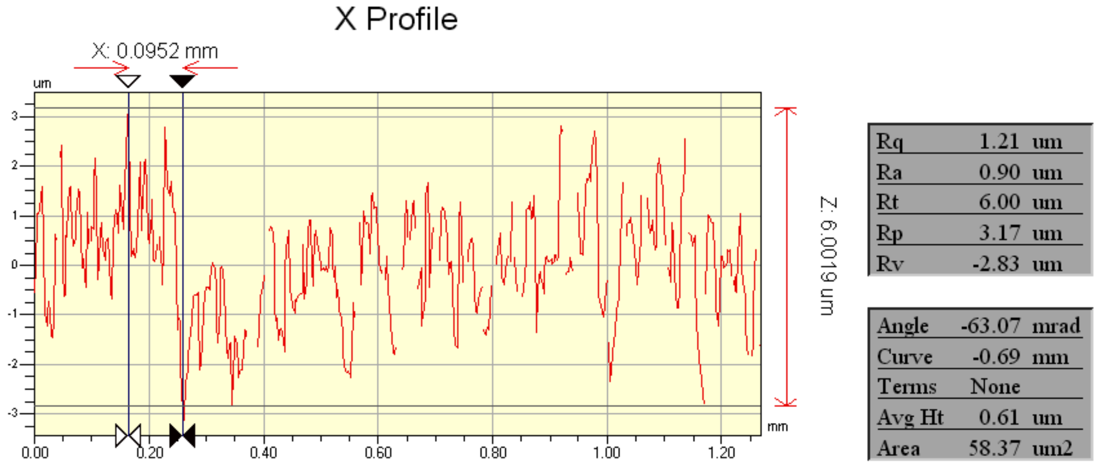

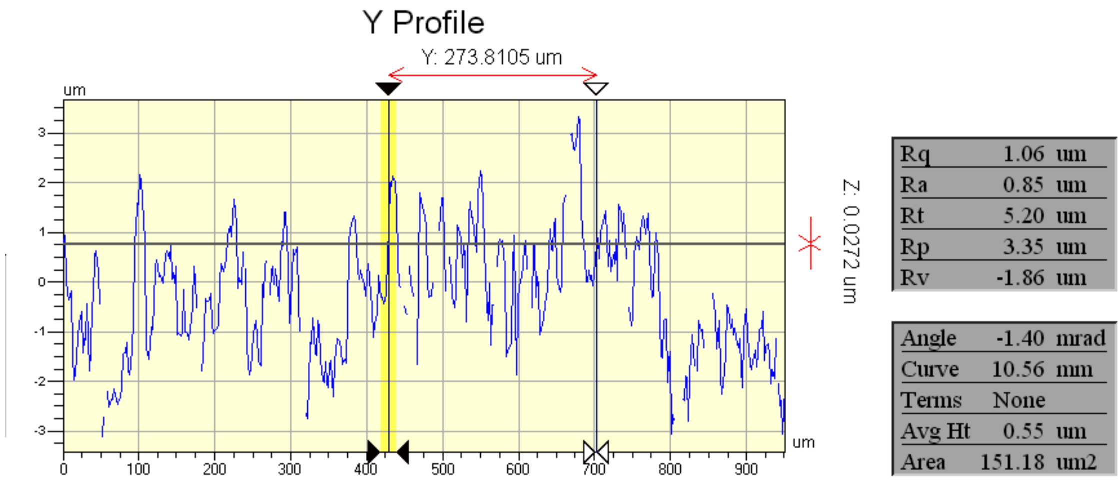

Figure 5-18 Two-dimensional topography of the surface of A.

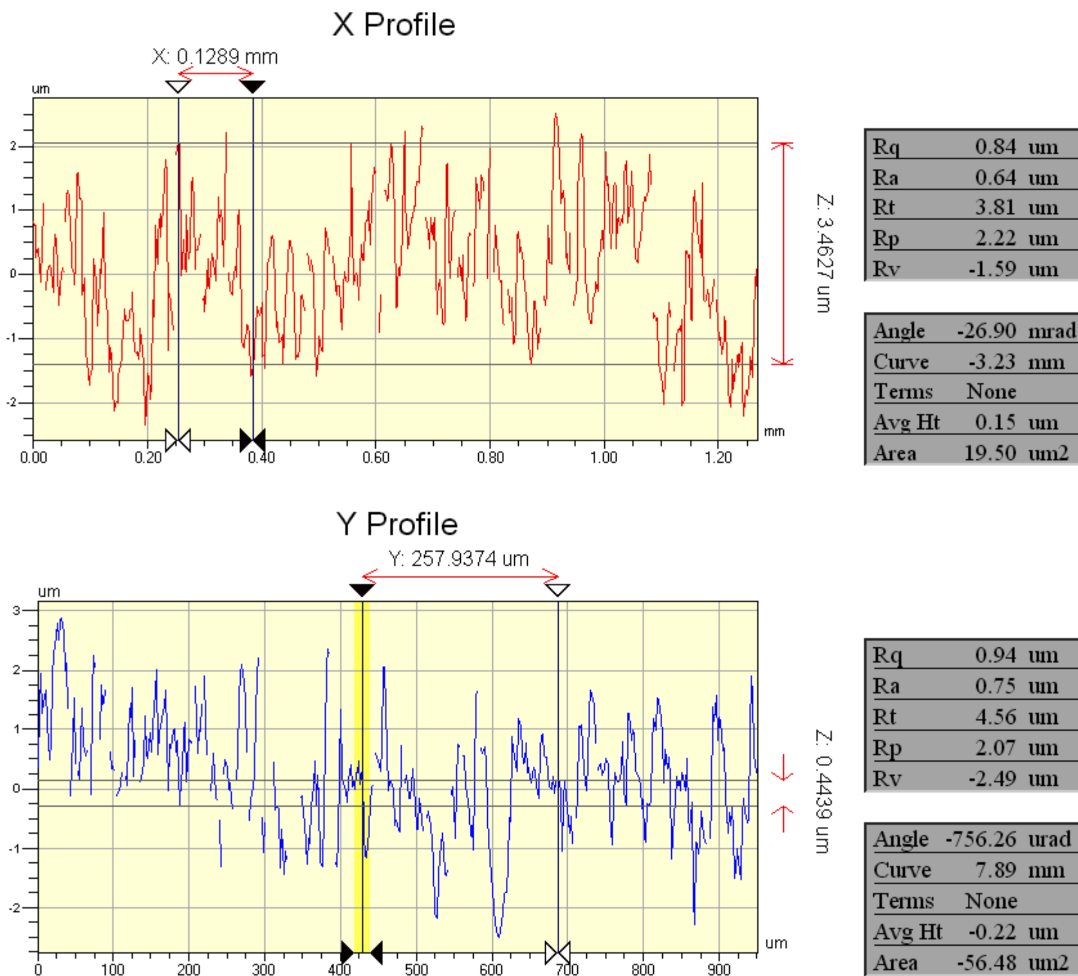

Figure 5-19 Two-dimensional topography of the surface of PA.

5.2.5. Ramman Spectroscopy

Raman spectroscopy was conducted in order to identify the phase structure of the titanium dioxide thin film. As expected from XRD results, the TiO_2 thin film on Ti substrate had an anatase phase, which causes major Raman bands on 144, 395, and 638 cm^{-1}. Positions of the Raman bands are the same as T for PT as well, as illustrated on Figure 5-20 and Figure 5-21.

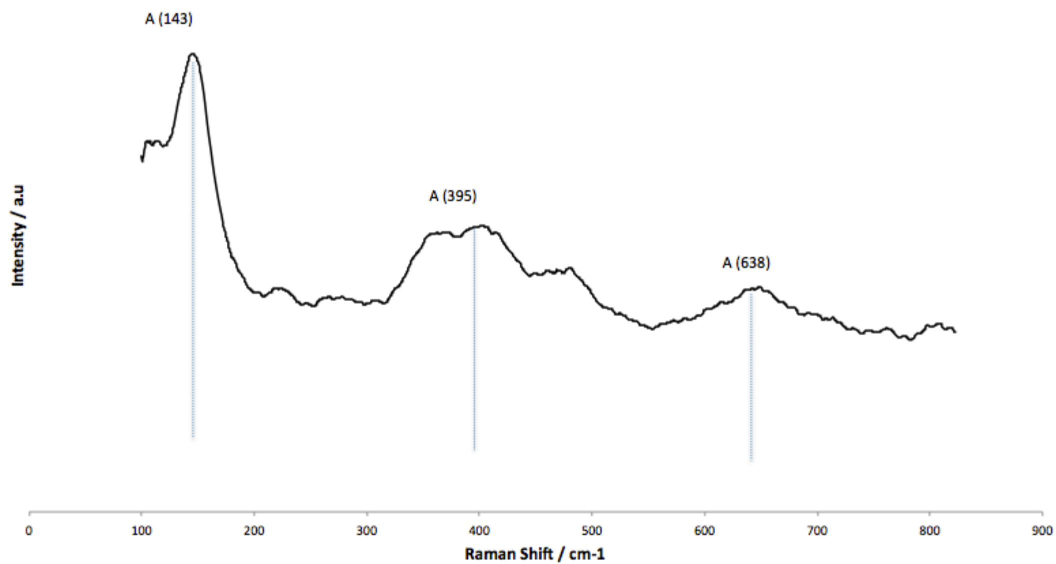

Figure 5-20 Raman spectra of TiO_2 thin film on flat Ti substrate (T).

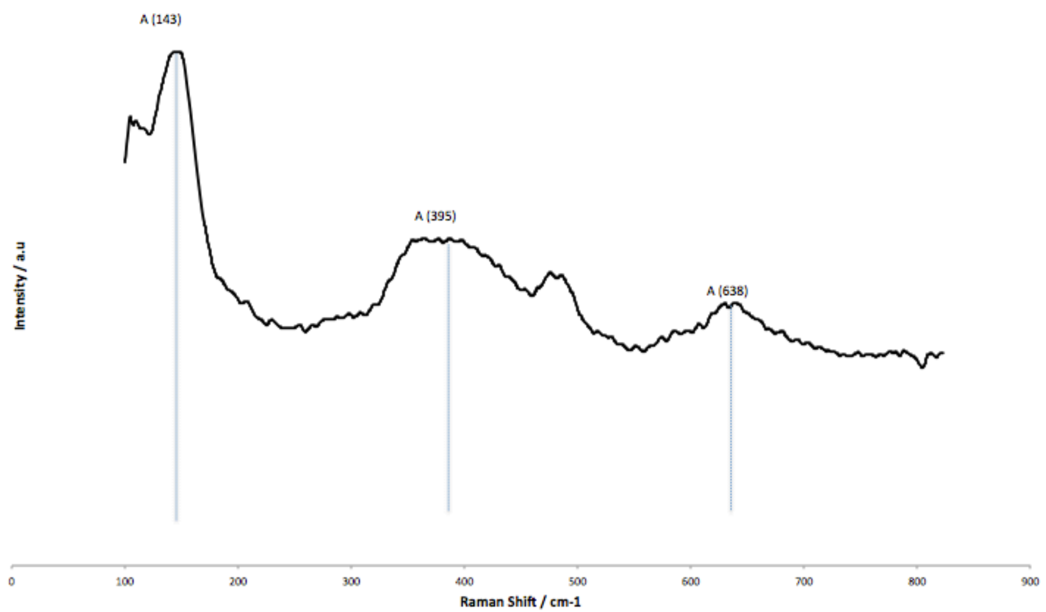

Figure 5-21 Raman spectra of TiO_2 thin film on EPP treated Ti substrate (PT).

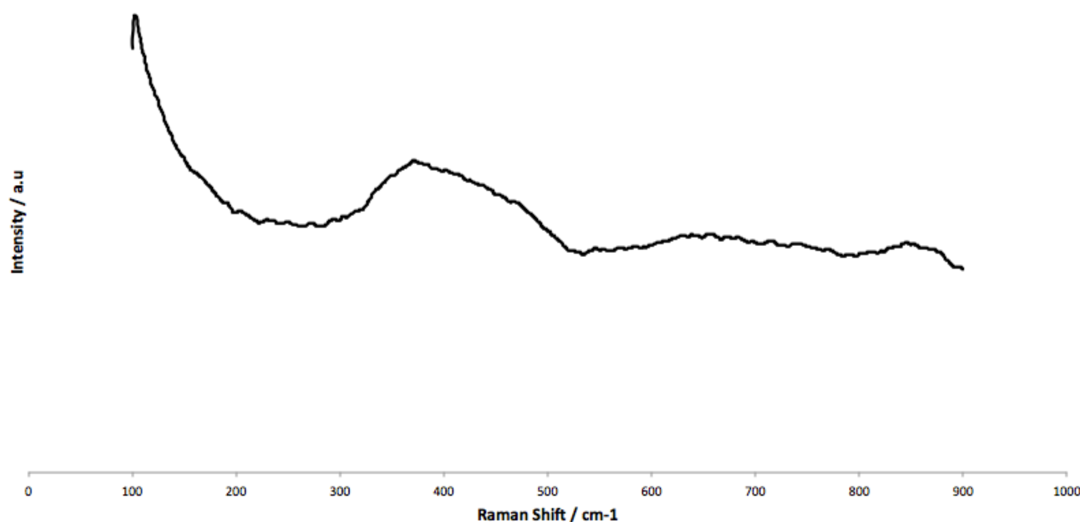

Figure 5-22 Raman spectra of TiO_2 thin film on Al substrate (A).

Figure 5-22 shows the Raman spectrum for the TiO_2 thin film on Al substrate. As it can be seen, there is not any distinct Raman band for TiO_2, either anatase or rutile phase except a very broad band at about 390 cm^{-1}. Although this Raman band could represent the existence of anatase phase on the thin film, but since the whole pattern does not follow the Raman spectra for anatase, the film is still considered to be amorphous. Therefore, Raman spectra reassure the XRD data, stating that the thin films grow amorphous on Al substrate.

5.3 Magnetron Sputtered Coatings

TiO_2 thin films were also deposited by magnetron sputtering. As described before, the TiO_2 film on Al substrate formed by plasma electrolytic oxidation did not show any photocurrent activity, which was due to the formation of Al_2O_3 during the EPP. Therefore, attempts were made to deposit a layer of TiO_2 on Al substrate by sputtering. TiO_2 thin films were also developed on EPP cleaned titanium and aluminum substrates by sputtering.

5.3.1. Photoelectrocurrent Measurement

Photocurrent activity of the deposited films was measured by a standard single-compartment, three-electrode electrochemical cell. The measurement was performed on the sputtered films on mirror finished and EPP treated Al and also EPP treated Ti substrate.

The produced photocurrent for TiO_2 thin film on flat Al substrate (SA) is shown in Figure 5-23. It can be observed that there is a relatively high photocurrent produced by this film and the current reached its plateau in fairly low voltages, which indicates the high conductivity of the thin film. Moreover, it can be detected that the film is stable up to voltages about 1.4. There is just a small dark current oxidation area, which probably is due to some electrochemical oxidation during the test.

Figure 5-24 illustrates the photocurrent activity of the TiO_2 sputtered thin film on the EPP patterned Al substrate (SPA). As it can be observed from the Linear-sweep photovoltammograms, the film is not stable and the current suddenly jumps up at relatively low voltages (about 0.45 V). This could be because of the substrate not being totally covered by the thin film. This causes the Al substrate to be exposed to the solution and get electrochemically oxidized during the experiment.

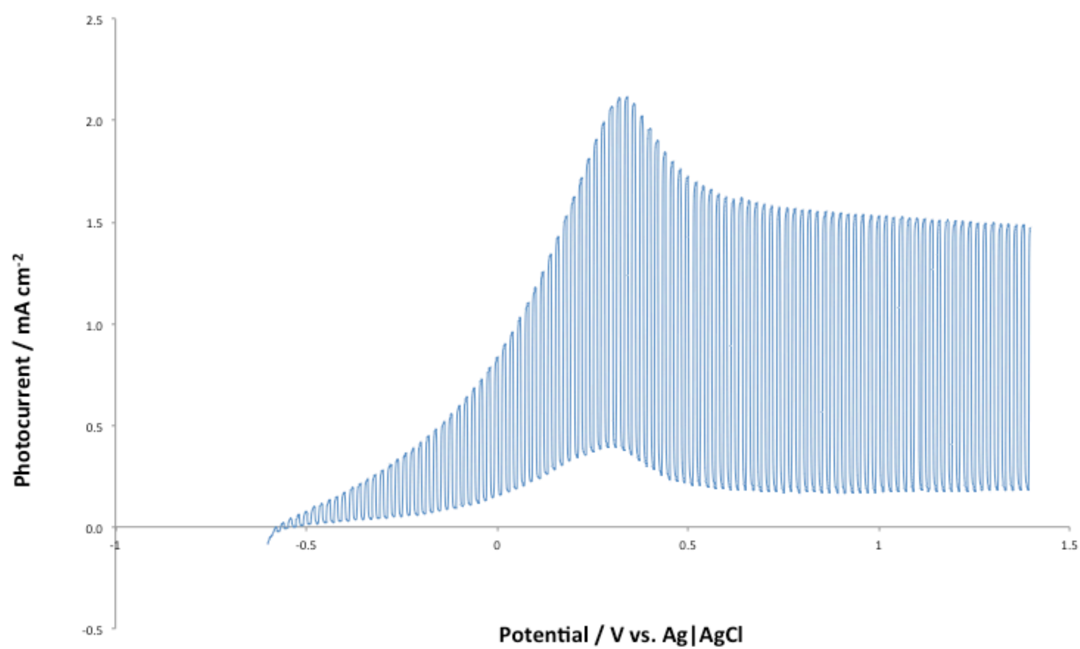

Figure 5-23 Linear-sweep photovoltammograms of sputtered TiO_2 thin film on flat Al substrate (SA).

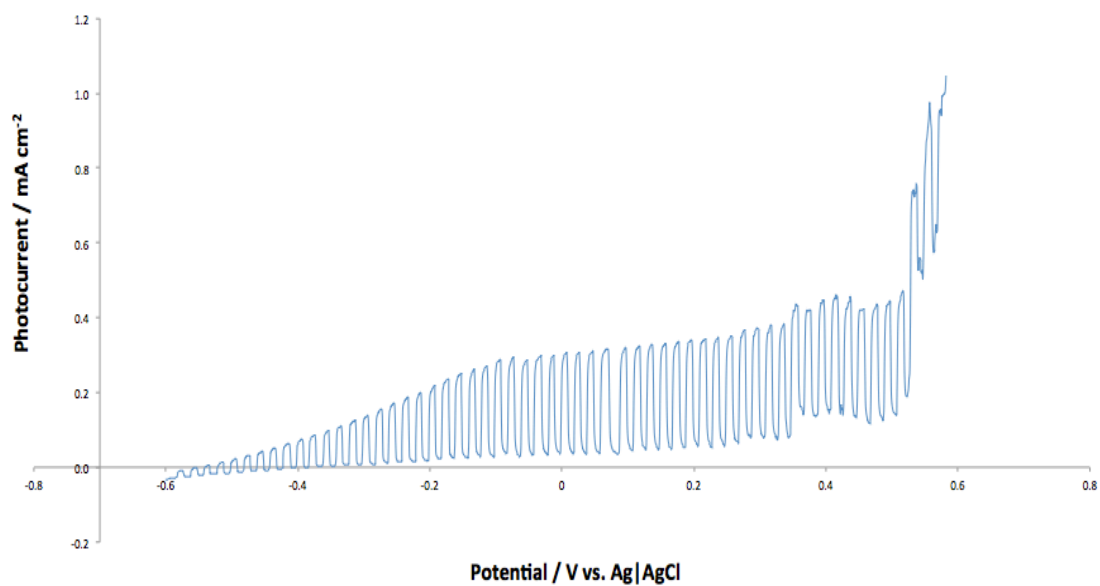

Figure 5-24 Linear-sweep photovoltammograms of sputtered TiO_2 thin film on EPP treated Al substrate (SPA).

The photoelectrocurrent genertated by sample SPT (TiO_2 film on EPP treated Ti substrate) is shown in Figure 5-25, illustrating a reasonably high photocurrent. There is no dark oxidation current detected showing the fact that the film has covered the whole substrate surface. Also, the film is stable at high voltages up to 1.4v, presenting that the thin film is electrochemically stable. Moreover, the stable photocurrent region (the plateau) starts at a comparatively low potential, which states a very high conductivity of the deposited film.

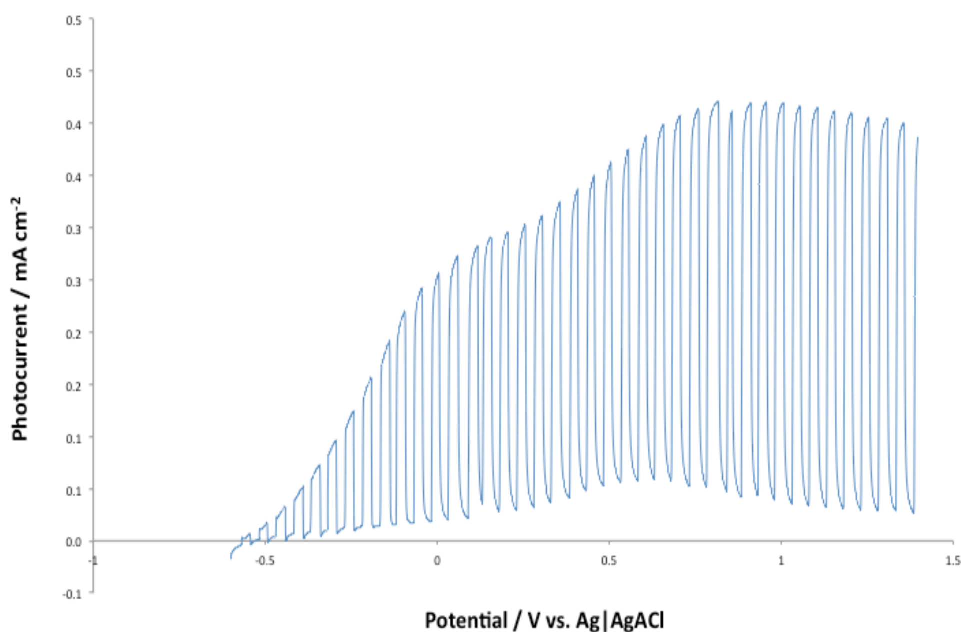

Figure 5-25 Linear-sweep photovoltammograms of sputtered TiO_2 thin film on EPP treated Ti substrate.

Comparing the created photocurrent by the PEO and sputtered TiO_2 thin film on Ti substrate, it can be concluded that the sputtered thin film can produce a much higher photocurrent than the PEO film as shown in Figure 5-26. As discussed before, the TiO_2 thin film created by sputtering has a nanostructure and a very high quality. The film is also much more conductive than the one deposited by PEO method.

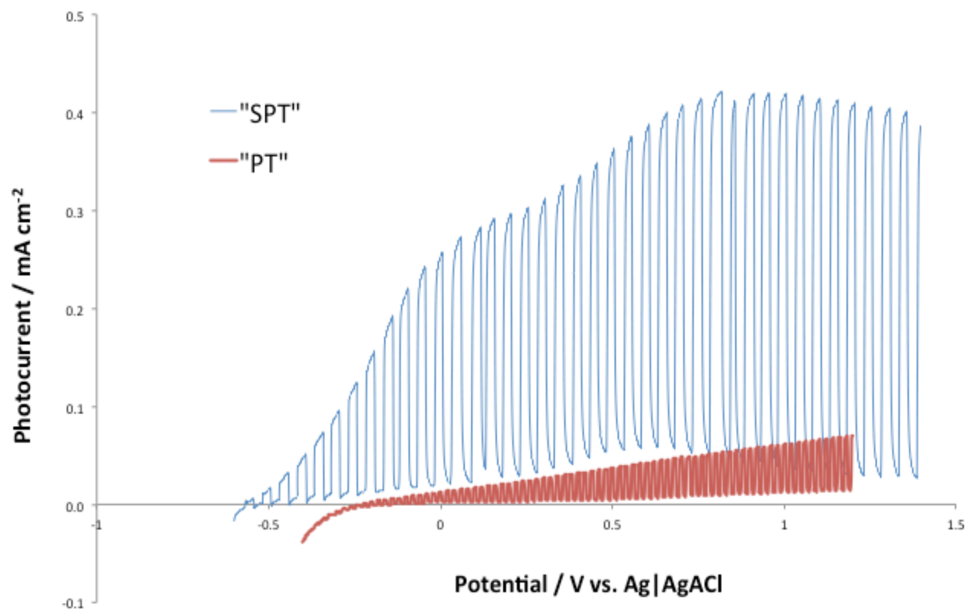

Figure 5-26 Linear-sweep photovoltammograms of sputtered and PEO TiO_2 thin film on Ti substrate.

5.3.2. EDS

The EDS is an essential tool that helps the determination of elements present at the near surface region. It's more of a qualitative technique rather than quantitative. Figure 5-27 and show the atomic percent of each element on the TiO_2 thin film deposited on flat Al surface by DC sputtering.

As listed in Table 5.1, there exists about 26% of titanium versus 52% of oxygen in the thin film, which indicates that the deposited film is close to stoichiometrically TiO_2. It is worth mentioning that the EDS analysis was performed with only 15 kV of accelerating voltage. Therefore, the beam did not penetrate all the way through the substrate and the data is mainly from shallow region.

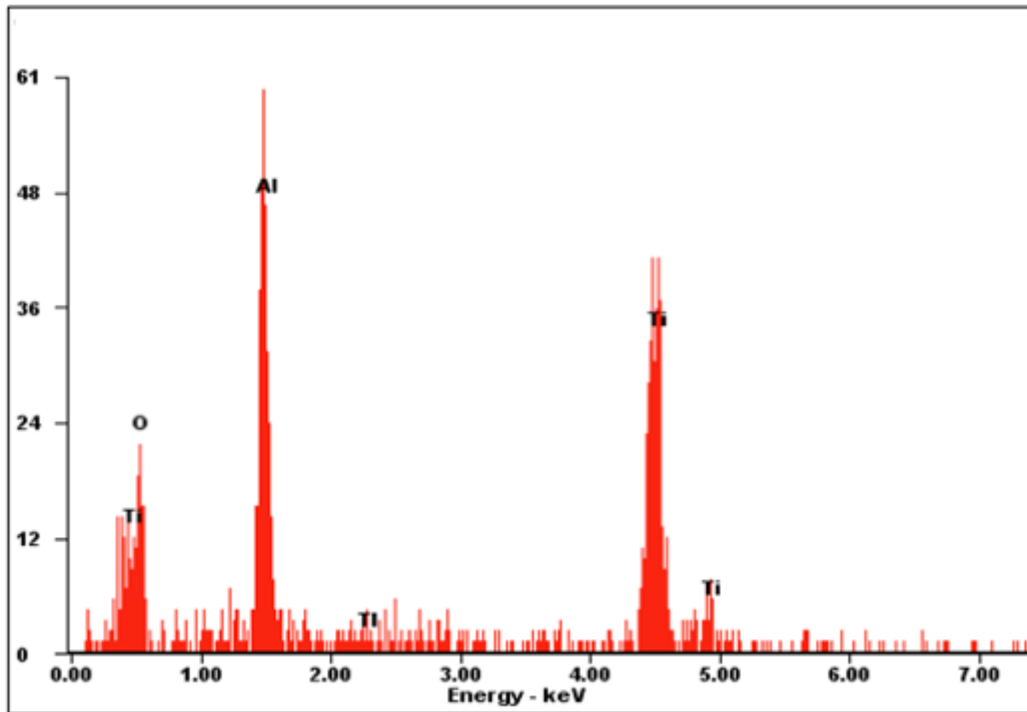

Figure 5-27 EDS spectra of TiO_2 thin film on Al substrate.

Table 5-1 Atomic and Weight Percent of Each Element in TiO_2 Thin Film

Element	Wt %	At %
O K	30.03	51.41
AlK	21.17	21.49
TlM	01.83	00.24
TiK	46.97	26.86

5.3.3. TEM

The microstructure of the sputtered thin film was studied by HRTEM. Figure 5-28 shows the TEM images of the thin film in different magnifications. As it can be perceived from the TEM images, there are just some small areas of crystalline phases in the film and the grain size of the deposited film is about 5 nanometers.

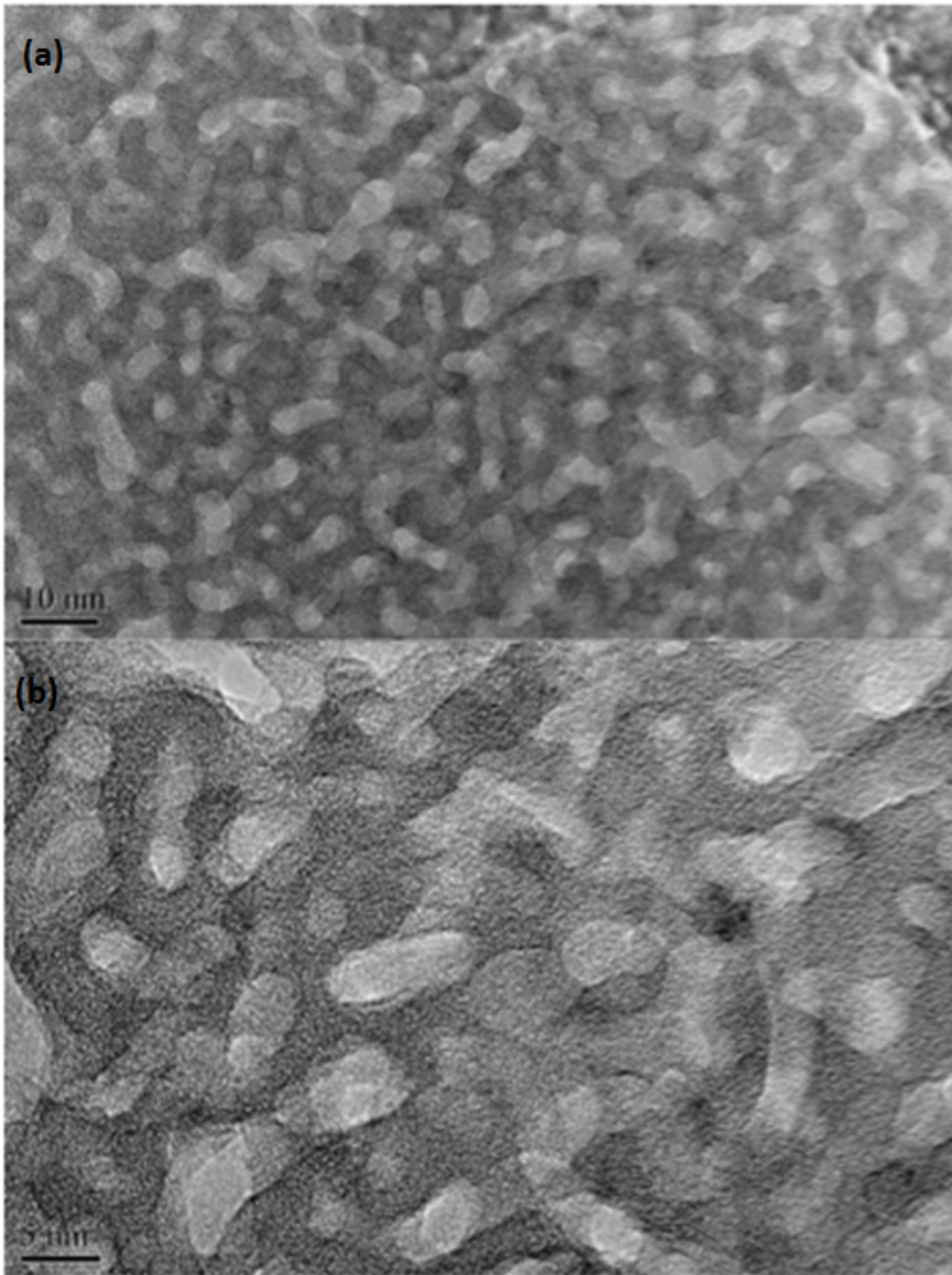

Figure 5-28 TEM micrograph of the sputtered TiO_2 thin film.

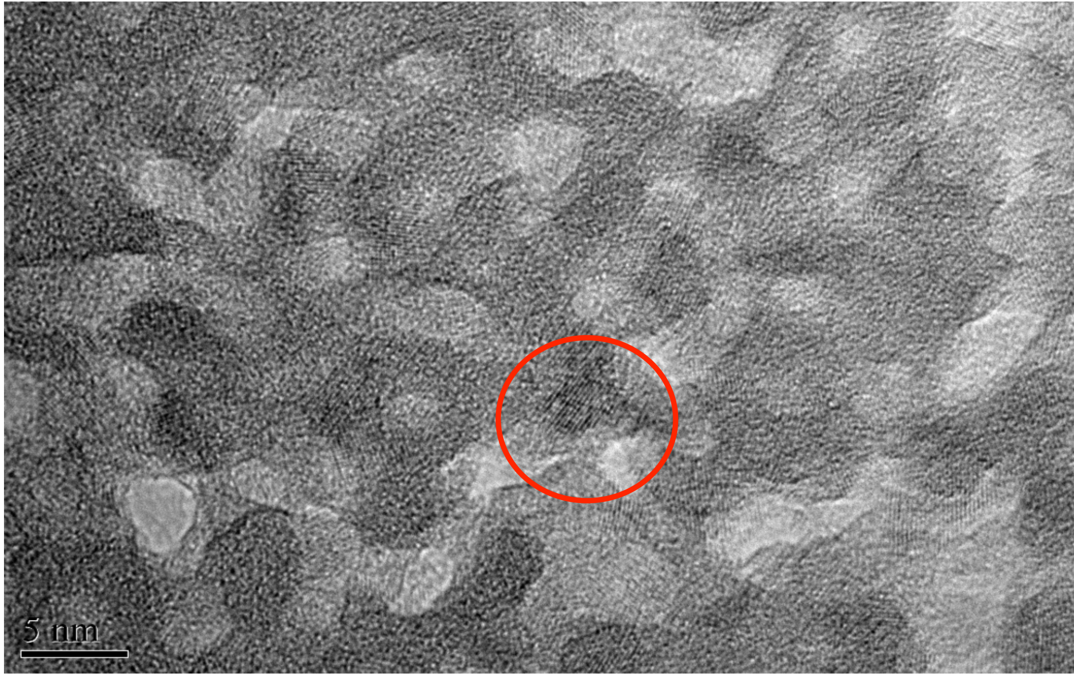

Figure 5-29 High resolution TEM image of the sputtered TiO_2 thin film.

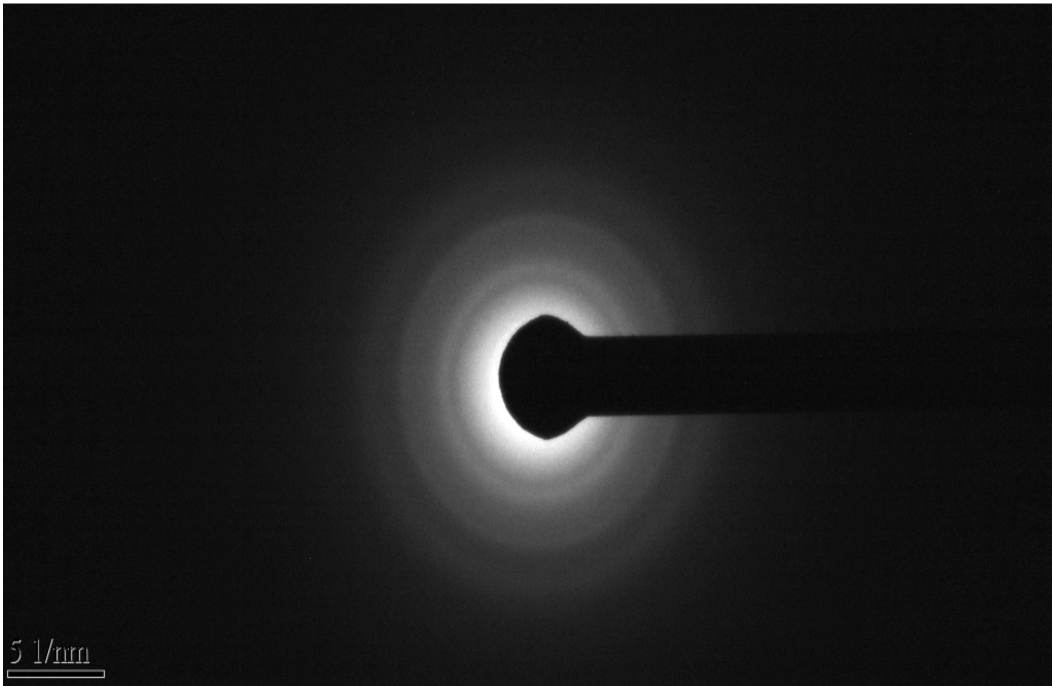

Figure 5-30 TEM ring pattern of the sputtered TiO_2 thin film on amorphous carbon.

As illustrated in the electron diffraction pattern of the sputtered thin film (Figure 5-30), there is some amount of crystalline on the deposited film due to the observation of diffraction rings. Based on the ring pattern and also the TEM micrograph, it can be stated that the deposited thin film is not fully crystalline but it has some crystalline regions along with amorphous phase. Moreover, the continuous nature of the rings confirms the very small grain size of the film.

In order to have a crystalline thin film, the same sputtered sample was annealed at 450°C for 2 hours. Since anatase is a not a stable phase in temperatures above 500°C, annealing temperature was selected to be 450°C so as for the TiO_2 thin film not to transform into the rutile phase. Figure 5-31 shows the electron diffraction pattern of the sputtered thin film after annealing. As it can be observed from the ring patterns, more sharp rings could be detected, which indicates the higher crystallinity of the film after annealing. However, it is still hard to determine whether the film is in anatase or rutile phase.

Figure 5-32 shows the high resolution TEM image of the sputtered thin film after annealing at 450°C for 2 hours. Comparing the two high resolution TEM images before and after annealing (Figure 5-29 and Figure 5-32) shows that the zones of the crystalline TiO2 increased after annealing. Other than that, Figure 5-32 indicates that the grain size of the thin film increased in comparison to the original sputtered film.

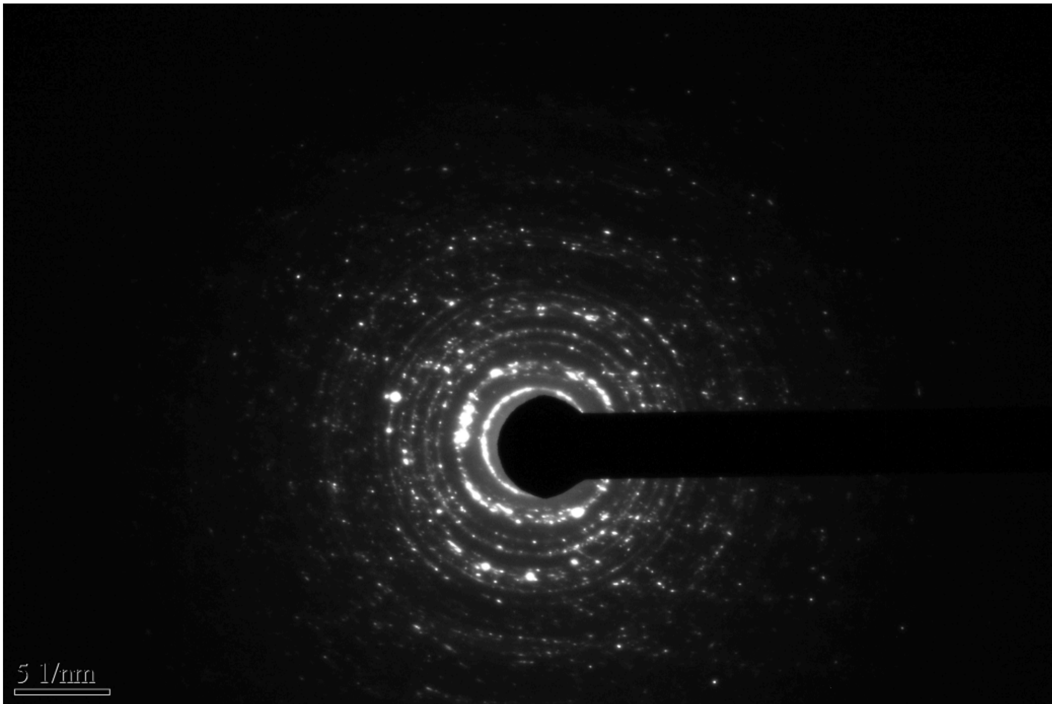

Figure 5-31 thin film on amorphous carbon after annealing at 450°C for 2 hours.

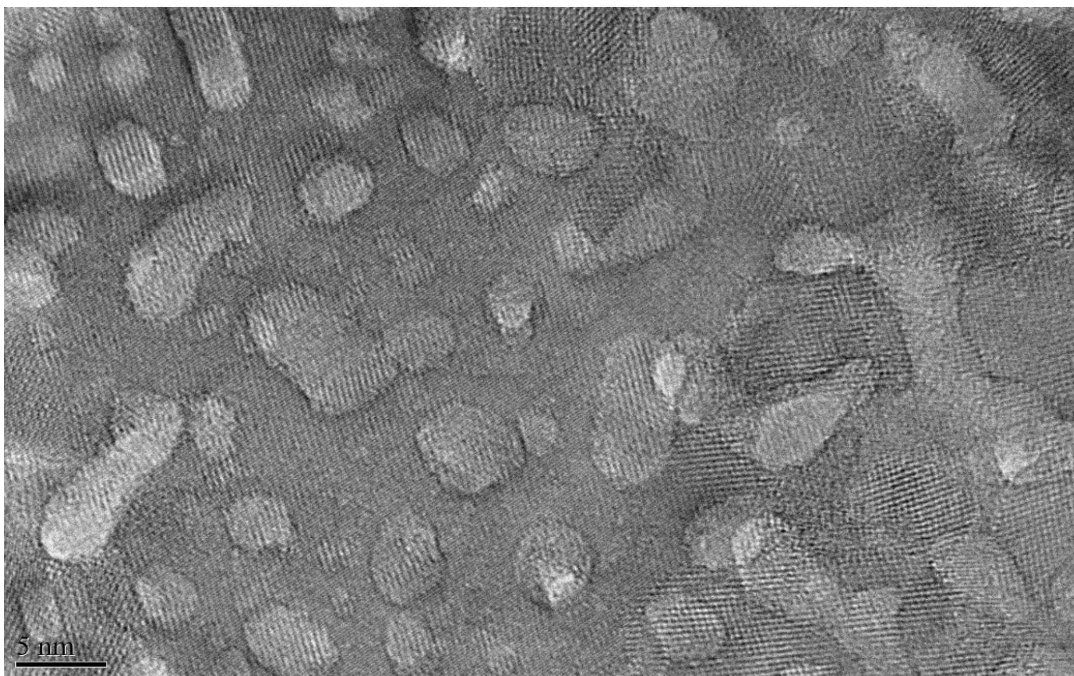

Figure 5-32 High resolution TEM image of the sputtered TiO_2 thin film after annealing at 450°C for 2 hours.

Table 5-2 Anatase and Rutile D-Spacing

Anatase D-Spacing (A)	Rutile D-Spacing (A)	TEM D-Spacing
3.51	4.13	3.533568905
2.43	3.24	2.789400279
2.37	3.07	2.554278416
2.33	2.68	2.34741784
1.89	2.6	1.974333662
175	2.37	1.863932898
1.7	2.29	1.699235344
1.66	2.26	1.455604076
1.49	2.06	
1.48	2.05	
1.36	2	
1.33	1.91	
1.28	1.88	
1.26	1.75	
1.25	1.72	
1.21	1.65	
1.18	1.64	
1.17	1.62	
1.16	1.6	
	1.58	
	1.55	
	1.53	
	1.51	
	1.45	
	1.44	
	1.43	
	1.42	
	1.39	
	1.38	
	1.37	
	1.14	
	1.13	
	1.12	
	1.11	
	1.1	

Figure 5-33 shows the photoelectrocurrent generated by the annealed film. As it can be seen, the film is totally stable and no dark current is observed during the photocurrent measurement, which means no electrochemical oxidations occurs during the measurement. The film is still fully conductive and the smooth increase of the current indicates the high quality of the film after annealing.

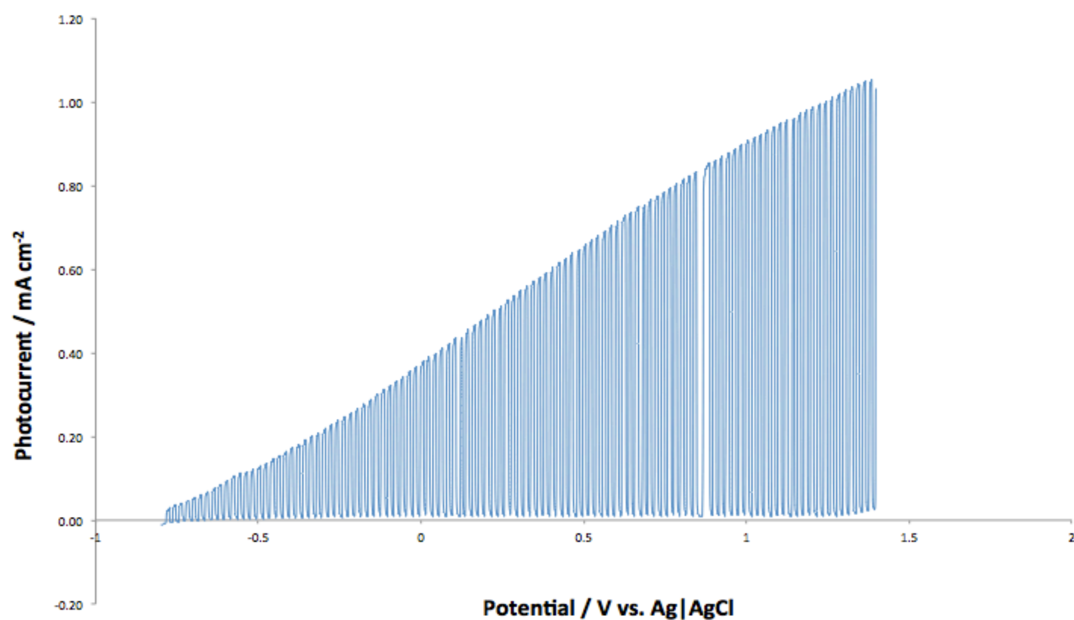

Figure 5-33 Linear-sweep photovoltammograms of sputtered Al substrate after annealing at 450°C for 2 hours.

However, the generated photocurrent of the annealed film is not as high the original sputtered film. This error could be due to the different deposition condition of the sputtered films.

CHAPTER 6

CONCLUSIONS

The following conclusions can be drawn from the present study:

- Using PEO technique, anatase was deposited on Ti and Amorphous TiO_2 was deposited on the Al substrate. The thickness of PEO deposited thin films varies between 6-10 μ.
- Photoelectrocurrent generated by TiO_2 thin films on Ti by PEO process increases by increasing the roughness of the substrate; however, the overall photocurrent remained low (about 0.1 $mA.cm^{-2}$).
- TiO_2 thin films on Al substrate by PEO method do not show any photoelectrocurrent activity because of the formation of aluminum oxide layer during the process.
- TiO_2 thin films with a very fine nanostructure were deposited on Ti and Al substrates using DC magnetron sputtering. The sputtered thin films show a photocurrent of 2 $mA.cm^{-2}$, which is considered as a high value for TiO_2 thin films.

REFERENCES

1. P. Chu, S. W, K. Chen, J. He, A. Yerokhin, A. Matthews, Thin Solid Films 519 (2010) 1723.
2. X. Li, K. Lva, K. Denga, J. Tanga, R. Sua, J. Suna, L. Chena, Materials Science and Engineering A 158 (2009) 40.
3. M. Kitano, M. Matsuoka, M. Ueshima, M. Anpo, Applied Catalysis A 325 (2007) 1.
4. P.J. Chu, A.L. Yerokhin, A. Leyland, A.Matthews, J.L. He, The International Conference on Metallurgical Coatings and Thin Films (ICMCTF), GP-6, Advanced Surface Engineering Division of the AVS, San Diego, California, USA, April 25–May 2 2009, p. 99.
5. J. Sun, Y. Wang, R. Sun, S. Dong, Material Chemistry and Physics 115 (2009) 303.
6. G.A. Battiston, R. Gerbasi, M. Porchia, A. Morigo, Thin Solid Films 239 (1994) 186.
7. P. Lobl, M. Huppertz, D. Mergel, Thin Solid Films 251 (1994) 72.
8. H. Tian, J. Ma, K. Li, J. Li, Materials Chemistry and Physics 112 (2008) 47.
9. H. Oh, J. Lee, Y. Kim, S. Suh, J. Lee, C. Chi, Materials Chemistry and Physics 109 (2008) 10.
10. M. Pourmand, N. Taghavinia, Materials Chemistry and Physics 107 (2008) 449.
11. M.R. Bayati, F. Golestani-Fard, A.Z. Moshfegh, Materials Chemistry and Physics 120 (2010) 582.
12. R. Suryanarayanan, Plasma Spraying: Theory and Applications, World Scientific (1993).
13. C. Cionea, "Microstructure Evaluation of Surface Layers During Electrolytic Plasma Processing", University of Texas at Arlington, Dissertation (2010).
14. X. Zhao, X. Liu, C. Ding, P. Chu, Surface and Coatings Technology 200 (2006) 5487.
15. T. Deguchi, K. imai, H. Matsui, M. Iwasaki, H. Tada, S. Ito, Journal of Materials Science 36 (2001) 4723.
16. A. Gunterschultze, H. Betz, Elecrolytkondensatoren, Krayn, Berlin (1937).
17. A. L. Yerokhin, X. Nie, A. Leyland, A. Mattews, S. J. Dowey, Surface and Coating Technology 122 (1999) 73.
18. http://farside.ph.utexas.edu/teaching/plasma/lectures/lectures.html
19. M.P. Brenner, D. Lohse, Physics Review Letters 21 (2008) 14505.

20. P.S. Epstein, M.S. Plesset, Journal of Chemical Physics 18 (1950) 1505.
21. A. Luzar, D. Bratko, Journal of Physical Chemistry B 109 (2005) 22545.
22. A. Poynor, Physics Review Letters 97 (2006) 266101.
23. A.L. Yerokhin, Electrophysical and Electrochemical Treatment of Materials, TulGU, Tula, 30, in Russian, (1996).
24. P. Gupta, G. Tenhundfeld, E.O. Daigle, D. Ryabkov, Surface and Coatings Technology 201 (2007) 8746.
25. A.L. Yerokhin, L. O. Snizhko, N. L. Gurevina, A. Leyland, A. Pilkington, A. Matthews, Journal of Physics D: Applied Physics, 36 (2003) 2110.
26. Y.M. Chen, Cavitation Erosion, ASM Handbook vol. 11, Metals Park, Ohio, (2003).
27. E.I. Meletis, X. Nie, F.L. Wang, J.C. Jiang, Surface and Coatings Technology 150 (2002) 246.
28. P. Gupta, G. Tenhundfeld, E.O. Daigle, P.J. Schilling, Surface and Coatings Technology 200 (2005) 1587.
29. P. Gupta and G. Tenhundfeld, Plating and Surface Finishing 92 (2005) 48.
30. P. Gupta, G. Tenhundfeld, E.O. Daigle, D. Ryabkov, and B. Calliham, Wire & Cable Technology International, XXXI, (2003) 52.
31. R. F. Bunshah, “Handbook of Deposition Technologies for Films and Coatings”, Noyes Publication, Second Edition (1949).
32. D. S. Rickerby, A. Matthews, “Advanced Surface Coatings: A Handbook of Surface Engineering”, Blackie Glasgow and London (1991).
33. D. Ren, Y. Zou, C. Zhan, N. Huang, Journal of Korean Physical Society, 58 (2011) 883.
34. P. Singh, Physica B 405 (2010) 1258.
35. Y. Ju, L. Li, Z. Wu, Y. Jiang, Energy Procedia 12 (2011) 450.
36. I. Hotov, A. Pullmannov, M. Predanocy, J. Hotov, V. Rehacek, T. Kups, L. Spiess, Journal of Electrical Engineering, 60 (2009) 354.
37. S. Boyadzhiev, V. Georgieva, M. Rassovska, Journal of Physics: Conference Series 253 (2010) 012040.
38. F. Meng, X. Song, Z. Sun, Vacuum 83 (2009) 1147.
39. C. Heo, S.Lee, J. Boo, Thin Solid Films 475 (2005) 183.
40. J. A Turner, “Photoelectrochemical Water System for H_2 Production”, National Renewable Energy Lab (2011).
41. N. R. de Tacconi, C. R. Chenthamarakshan, G. Yogeeswaran, A. Watcharenwong, R. S. de Zoysa, N. A. Basit, K. Rajeshwar, Journal of Physical Chemistry B 110 (2006) 25347.

42. A. L. Linsebigler, G. Lu, and J. T. Yates, “Photocatalysis on TiOn Surfaces: Principles, Mechanisms, and Selected Results”, Chemical Reviews 95 (1995) 735.
43. R. W. Matthews, Journal of Catalysis 113 (1988) 549.
44. Burdett, J. K., Inorganic Chemistry 24 (1985) 2244.
45. J. K. Burdett, T. Hughbands, J. M. Gordon, J. W. Richardson, J. V. Smith, Journal of American Chemical Society 109 (1987) 3639.
46. A. Fahmi, C. Minot, B. Silvi, M. Causa, Physical Review B 47 (1993) 11717.
47. V. Zwilling, M. Aucouturier, E. Darque-Ceretti, Electrochimica Acta 45 (1999) 921.
48. D. Gong, C. Grimes, O. K. Varghese, W. Hu, R. S. Singh, Z. Chen, E. C. Dickey, Journal of Material Research 16 (2001) 3331.
49. O. K. Varghese, M. Paulose, K. Shankar, G. K. Mor, C. A. Grimes, Journal of Nanosience and Nanotechnology 5 (2005) 1158.
50. K. Rajeshwar, In Encyclopedia of Electrochemistry, Germany, Vol. 6, Chapter 1, 1-53 (2002).
51. G. Hodes, I. D. J. Howell, L. M. Peter, Journal of Electrochemical Society 139 (1992) 3136.
52. A. Hagfeldt, M. Gra¨tzel, Chemical Reviews 95 (1995) 49.
53. A. Fahmi, C. Minot, B. Silvi, M. Causa, Physical Reviews B 47 (1993) 11717.
54. J. A. Turner, Journal of Chemical Education 60 (1983) 327.
55. A. G. Milnes, D. L. Feucht, Heterojunctions and Metal Semiconductor Junctions Academic Press, New York and London, Chapter 5, p. 139 (1973).
56. L. Palmisano, A. Sclafani, Heterogeneous Photocatalysis, John Wiley & Sons 111 (1997).
57. M. R. Hoffmann, S. T. W. Martin, W. Choi, D. W. Bahnemann, Chemical Reviews 95 (1995) 69.
58. C. R. Chenthamarakshan, N. R. Tacconi, R. Shiratsuchi, K. Rajeshwar, International Journal of Electrochemical Science 553 (2003) 77.
59. N. R. de Tacconi, C.R. Chenthamarakshan, G. Yogeeswaran, A. Watcherenwong, R. S. de Zoysa, N. A. Basit, and K. Rajeshwar, Journal of Physical Chemistry B 110 (2006) 25347.
60. P. J. Hazarika, “Synthesis, Structure And Characterization of Silver Doped Diamond Like Carbon Thin Films”, University Of Texas At Arlington, Dissertation (2007).
61. P. J. Caber, Applied Optics 32 (1993) 3438.
62. B.D. Cullity and S.R. Stock, Elements of X-ray Diffraction, Prentice Hall, Upper SaddleRiver, NJ 07458, 399, (2001).

BIOGRAPHICAL INFORMATION

Aida Mehdinezhad Roshan was born in April 1989, in Babol, Iran. She received her bachelor degree in Materials Science and Engineering from Sharif University of Technology, Tehran, Iran in 2011. During her undergraduate studies, she had been involved with research projects mainly in the area of biomaterials. She has written her bachelor's thesis on hydroxyapatite coatings by plasma electrolytic oxidation, a novel coating technique for bio-implants. Right after completing her undergrad studies, she decided to pursue her masters at University of Texas at Arlington in September 2011. Her focal field of research as a graduate student was thin films in the Surface and Nano-engineering laboratory. These research projects explore different techniques such as plasma electrolytic oxidation and RF/DC sputtering systems as novel routes for processing and growing thin films, which have numerous applications ranging from form bio-ceramics to semiconductors and corrosion resistance. She is a candidate for the degree of Master of Science in Material Science and Engineering to be awarded in May 2013.